DOI: 10.1002/ejoc.200500510

The Ligand-Exchange Process of P–H_{apical} Phosphoranes and the Thermal Formation and Pseudorotation of Anti-Apicophilic Spirophosphoranes

Satoshi Kojima,[a] Kazumasa Kajiyama,[a] Masaaki Nakamoto,[a] Shiro Matsukawa,[a] and Kin-ya Akiba*[a][‡]

Keywords: Anti-apicophilic compounds / Hypervalent compounds / Kinetics / Phosphoranes / Pseudorotation

Monocyclic P–H_{apical} phosphoranes **10** bearing a ring-opened Martin ligand are formed upon treatment of the P–$H_{equatorial}$ spirophosphorane **7** with more than 2 equiv. of alkyllithium compounds. A ligand-exchange process of these phosphoranes **10** involving the interconversion of the bidentate Martin ligand with the monodentate Martin ligand was found to proceed, probably through a hexacoordinate phosphorus atom. Heating of **10** in nondonating solvents furnished alkylspirophosphoranes **5**, whereas heating of **10** in donor solvents led to the formation of anti-apicophilic phosphoranes **6**, a new class of phosphoranes in which the less apicophilic carbon substituent occupies an apical position and the more apicophilic oxygen atom occupies an equatorial position. These phosphoranes **6** were found to completely convert into their energetically more stable $C_{equatorial}$,O_{apical} stereoisomers **5** upon heating. On the basis of kinetic examinations of the cyclization process of **10**, the formation of **6** can be rationalized by the enhanced nucleophilicity of the hydroxy group in the donor solvents. The isomer **5b** was estimated to be more stable than **6b** (R = *n*Bu) by 12 kcal mol^{-1} from kinetic studies on the pseudorotation of **6b** to **5b**. This is in good agreement with theoretical calculations with analogous **5a** and **6a** (R = Me), which estimate the difference in energy to be 14.1 kcal mol^{-1}.

Introduction

Stable pentacoordinate 10-P-5[1] phosphoranes have served as model compounds for intermediates in reactions involving the phosphoryl unit in biological systems.[2] Phosphoranes usually assume trigonal-bipyramidal structures in which there are two distinctive groups of sites − the apical and the equatorial positions. The positional exchange of these stereochemically fluxional compounds is usually described in terms of Berry pseudorotation (BPR), which has its basis in bond bending and generally follows a low-energy process.[3,4] Because of the electron-rich nature of the hypervalent three-center,four-electron apical bond,[5] elements (substituents) more capable of stabilizing negative charge are preferred in these apical positions. Thus, the ability to stabilize this bond, known as apicophilicity, usually parallels the electronegativity of the elements (or substituents).[6] Several experimental[4,7,8] and theoretical[9] apicophilicity scales, mostly based on the relative barriers of pseudorotation, have been proposed in the past. Although apicophilicities are different according to their systems, the general consensus is that an oxygen atom is much more apicophilic than a carbon atom. Thus, a phosphorane having a mixture of oxygen and carbon substituents, and capable of undergoing pseudorotation, would naturally be expected to have a maximum number of oxygen atoms in the apical positions in the most stable stereoisomer(s) (**I**; Scheme 1). As for configurational isomers with an apical oxygen atom and an equatorial carbon atom reversed (**II**, **II′**), they have been assumed to exist as high-energy intermediates on the pseudorotation coordinate for interconversion of *P*-epimers of **I**. However, such species have never been observed simultaneously with **I**. This is understandable considering the fact that a rather large difference in energy is expected for them [empirical estimate: ca. 8.3 kcal mol^{-1};[10] theoretical values for cyclic phosphorane $PH_3(CH_2CH_2O)$: 7.77[11] and 2.4 kcal mol^{-1};[9c] for acyclic phosphorane PH_3CH_3OH:[12] 1.6 kcal mol^{-1}]. Furthermore, there is a question as to whether such species actually exist as stationary points on the pseudorotation reaction coordinate at all.[12]

One method of obtaining a phosphorane with an apical carbon atom in the presence of more electronegative heteroatoms would be by raising the intrinsic apicophilicity of the carbon substituent by introducing electron-withdrawing groups onto it. For example, for carbon and fluorine substituents the use of fluorinated carbon atoms has led to the observation of **1** in equilibrium with its equatorial CF_3 isomer by IR spectroscopy.[13] Another method would be to utilize ring strain (four- or five-membered bidentate li-

[a] Department of Chemistry, Graduate School of Science, Hiroshima University,
1-3-1 Kagamiyama, Higashi-Hiroshima 739-8526, Japan
[‡] Present address: Advanced Research Center for Science and Engineering, Waseda University,
3-4-1 Ohkubo, Shinjuku-ku, Tokyo 169-8555, Japan
E-mail: akibaky@waseda.jp
Supporting information for this article is available on the WWW under http://www.eurjoc.org or from the author.

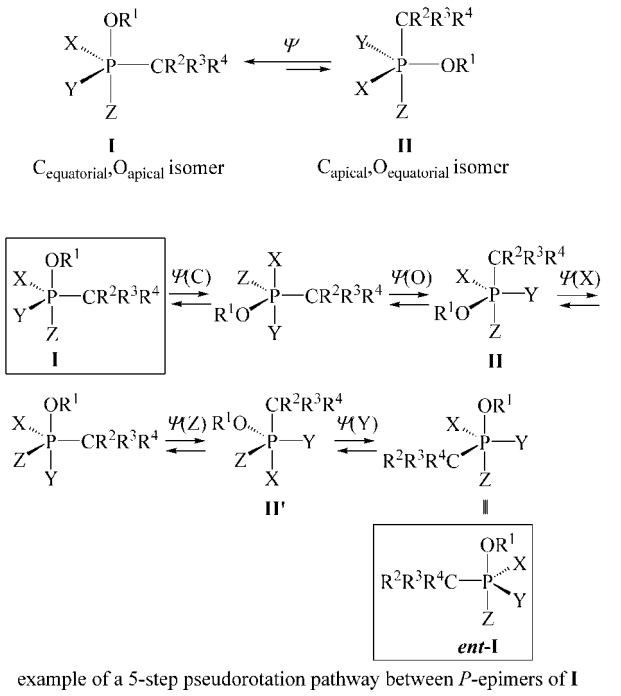

Scheme 1.

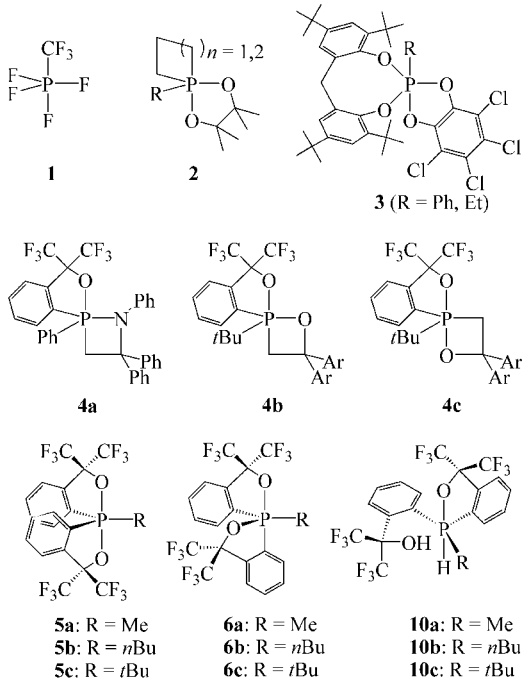

Figure 1.

gands), as in compound **2**, such that the bidentate ligands can only span an apical and an equatorial position (Figure 1).[14] There are a great many examples of this group of compounds.[4] Still another method would be to employ steric effects and ring strain together. Holmes and co-workers, for example, have prepared phosphoranes **3** with an apical carbon atom and equatorial oxygen atoms.[15] Here, the eight-membered ring is forced by the bulky *t*Bu groups and by the bond-angle effect to occupy two equatorial sites, while the five-membered ring is forced to occupy an apical and an equatorial site, thus making the monodentate alkyl group sit at the remaining apical position. As for carbon and nitrogen substituents, Kawashima and co-workers have found that **4a** is in equilibrium with its C$_{equatorial}$ stereoisomer by introducing a phenyl group at the nitrogen atom.[16] While all of these methods do indeed give unusual C$_{apical}$ rotamers, it can be said that the intrinsic apicophilicity of the elements has been altered by special factors.

By utilizing the Martin ligand,[17] we have recently achieved the isolation and characterization of the first anti-apicophilic phosphorane **6b**, which we define as a 10-P-5 phosphorane that is *P*-epimeric with, although less stable than, phosphorane **5b**, which has a configuration that fulfils the apicophilicity rules in terms of ordinary substituent electronegativity (Figure 1). In the case of **6b**, the less apicophilic carbon substituent occupies an apical position and the more apicophilic oxygen atom occupies an equatorial position (*O-cis*), while **5b**, which has an ordinary configuration with two apical oxygen atoms (*O-trans*), exists as the more stable isomer, as described in a preliminary report.[18] Evolving from this discovery, we later found that anti-apicophilic phosphoranes **6** can even be prepared at ambient temperature or lower by using I_2 as the oxidant.[19a] Phosphoranes **4b** and **4c**, which contain an oxaphosphetane ring, have also been prepared and characterized by us. Pseudorotation of the *O-cis* isomer **4b** to its *O-trans* isomer **4c** proved that, unlike **4a** and all other reported unusual C$_{apical}$ rotamers, the intrinsic element apicophilicities had not been altered.[19b] Furthermore, establishment of methods to obtain anti-apicophilic phosphoranes has allowed us to examine the difference in reactivity between isomeric phosphoranes of types **5** and **6**, and thus we have found that the latter anti-apicophilic phosphoranes are much more reactive towards nucleophiles than their *O-trans* isomers.[19c] In this paper, we present our kinetic examination of the thermal cyclization process of P–H$_{apical}$ phosphoranes **10** to give *O-cis* **6**, in conjunction with the pseudorotation process of **6**, and, based upon these results, we present a mechanistic rationale for the unique formation of **6**. We also describe the stereomutation properties of **10**, along with full details of the preliminarily reported results.

Results and Discussion

Formation of Monocyclic P–H$_{apical}$ Phosphoranes 10

During our investigation of the electrophilic substitution reactions of phosphoranide **8**, generated by deprotonation of P–H$_{equatorial}$ spirophosphorane **7**,[8,20] we noticed that when alkyllithium reagents were used as base, varying amounts of side products in which the alkyl group from the lithium reagent was incorporated, such as **5**, were obtained (Scheme 2). In order to form the product 10-P-5 phosphoranes from the dianionic species **9**, a subsequent oxidative process is required. We speculated that aqueous treatment of **9** had led to diprotonated species such as **10** and

subsequent cyclization with concomitant H_2 evolution gave the ultimate alkylspirophosphoranes **5**. In order to prove this assumption we set out to isolate the supposed intermediate **10**. When compound **7** was treated with more than 2 equiv. of RLi (R = Me, *n*Bu, *t*Bu) in diethyl ether and carefully treated with acid, monocyclic P–H_{apical} phosphoranes **10a** [R = Me; ^{31}P NMR ($CDCl_3$): δ = –51.9 ppm ($^1J_{P,H}$ = 276 Hz)], **10b** [R = *n*Bu; ^{31}P NMR ($CDCl_3$): δ = –34.4 ppm ($^1J_{P,H}$ = 273 Hz)], **10c$_{intra}$** [R = *t*Bu; ^{31}P NMR ($CDCl_3$): δ = –14.7 ppm ($^1J_{P,H}$ = 273 Hz)], and **10c$_{inter}$** [R = *t*Bu; ^{31}P NMR ([D$_6$]acetone): δ = –40.1 ppm ($^1J_{P,H}$ = 293 Hz)] were indeed found to form, along with varying amounts of the corresponding **5**. Judging from the similarity of the ^{1}H NMR patterns for the two species of **10c**, we assumed them to be isomers. Their actual identities − differing modes of solvation − were later revealed by X-ray analysis (vide infra). The characteristically small $^1J_{P,H}$ values ($^1J_{P,H}$ = 273 Hz) compared with that of **7** ($^1J_{P,H}$ = 729 Hz), in which the hydrogen atom is equatorial, indicated that the hydrogen atom is bonded to the phosphorus atom in the apical position, as already observed for **11**.[17c,21] Isomeric ring-opened phosphanes **12** that could be imagined to be in equilibrium with **10** were not observed, even though the presence of an alkyl group was expected to destabilize the monocyclic 10-P-5 phosphoranes **10**.

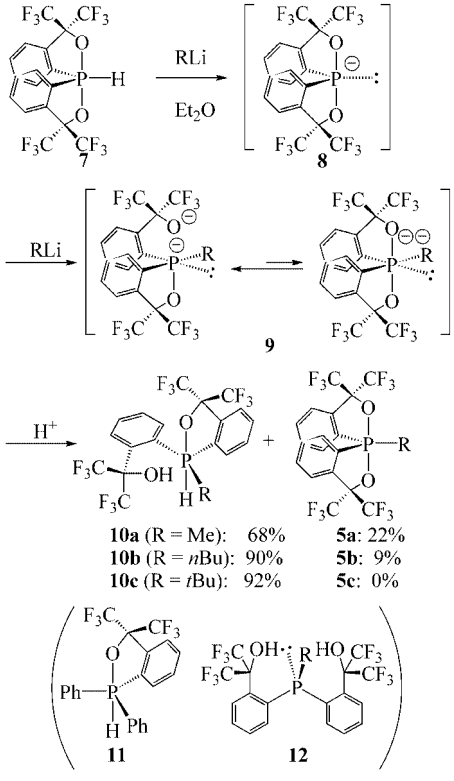

Scheme 2.

We have previously observed similar amphiphilic properties in a spirostiboranide that differs from **8** only in the central atom.[22,23] However, no intermediates analogous to **10** or **7** could be observed in the antimony series.

X-ray Structure of the P–H$_{apical}$ Phosphoranes 10

X-ray structural analyses of compounds **10a** (R = Me), **10b** (R = *n*Bu), **10c$_{intra}$** (R = *t*Bu), and **10c$_{inter}$** (R = *t*Bu) revealed that the former three have similar structures. In the case of compound **10c**, the different forms could be recrystallized independently by changing the solvent − hexane/CCl_4 for **10c$_{intra}$** and hexane/MeCN for **10c$_{inter}$**. The ORTEP plots of **10c$_{intra}$** and **10c$_{inter}$** are shown in Figure 2, with selected structural parameters for all four compounds given in Table 1. All of them assume a trigonal-bipyramidal structure, as evident from the sum of the three C–P–C angles in the projected equatorial plane (359.4–360.0°), with the hydrogen atom positioned apical, as expected. The common feature among **10a**, **10b**, and **10c$_{intra}$** is the presence of intramolecular hydrogen bonding between the apical oxygen atom and the O–H hydrogen of the monodentate Martin ligand. Possibly in order to accommodate this hydrogen bonding, the benzene ring of the monodentate Martin ligand is distorted, with a P1–C10–C15 angle of about 133° instead of 120°. On the other hand, **10c$_{inter}$** engages in intermolecular hydrogen bonding with an MeCN molecule. Thus, **10c$_{intra}$** is unsolvated and **10c$_{inter}$** is solvated. This is a rare example of a fully characterized pair of unsolvated and solvated forms due to different modes of hydrogen bonding and, incidentally, the first involving 10-P-5 phosphoranes that we are aware of. As a consequence of the *trans* influence, the apical P1–O1 bond (1.91–1.95 Å) is longer for all four (vide infra) than for other phosphoranes bearing the Martin ligand, such as spirophosphorane **5**, in which it is about 1.77 Å, when the opposite element is oxygen.[19c] Furthermore, it seems that intramolecular hydrogen bonding in **10a**, **10b**, and **10c$_{intra}$** weakens and elongates the apical P–O1 bond even further, as evident from the values of 1.914, 1.954, and 1.919 Å for **10a**, **10b**, and **10c$_{intra}$**, respectively, compared with 1.837 Å for **10c$_{inter}$**. The O2–P1 distance in **10c$_{inter}$** (2.84 Å) is shorter than that in **10c$_{intra}$** (3.10 Å) and the sum of the van der Waals radii of the two atoms (3.3 Å).[24] The oxygen atom is also oriented so that a lone pair can be projected to face and weakly interact with the phosphorus atom. This coincides with the ^{31}P

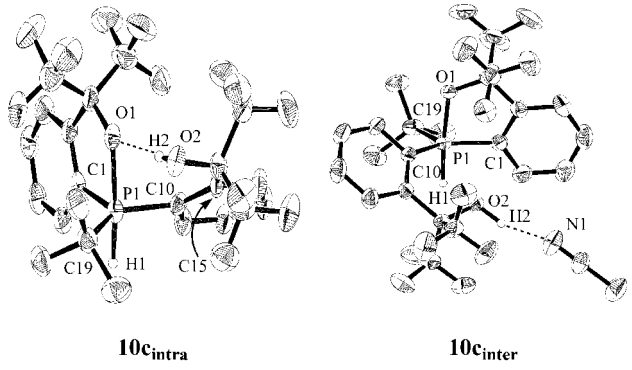

10c$_{intra}$ **10c$_{inter}$**

Figure 2. ORTEP drawings of **10c$_{intra}$** and **10c$_{inter}$** showing the thermal ellipsoids at the 30% probability level. All the hydrogen atoms other than P1–H1 and O2–H*2* have been omitted for clarity. The broken lines denote hydrogen bonding.

chemical shift of **10c$_{inter}$** [δ_P ($CDCl_3$) = –43.0 ppm] being at higher field (more electron-rich) than that of **10c$_{intra}$** [δ_P ($CDCl_3$) = –14.7 ppm].

Table 1. Selected bond lengths [Å] and angles [°] for **10a**, **10b**, **10c$_{intra}$**, and **10c$_{inter}$**.

	10a	10b	10c$_{intra}$	10c$_{inter}$
P1–H1	1.190(1)	1.450(1)	1.371(2)	1.371(1)
P1–O1	1.914(3)	1.954(2)	1.919(8)	1.837(2)
P1–C1	1.812(5)	1.811(3)	1.82(1)	1.815(4)
P1–C10	1.838(4)	1.847(3)	1.886(10)	1.847(4)
P1–C19	1.808(5)	1.814(3)	1.86(1)	1.869(4)
O2–H2	0.947(3)	0.987(2)	0.586(8)	1.025(2)
O1–H2	1.661(3)	1.653(2)	2.003(6)	
N1–H2				1.783(5)
P1–O2	3.098(4)	3.071(3)	3.142(8)	2.827(3)
O1–P1–H1	174.5(1)	176.0(1)	173.4(2)	174.0(1)
O1–P1–C1	83.6(2)	83.5(1)	83.1(4)	84.8(1)
O1–P1–C10	88.0(2)	87.6(1)	91.6(4)	88.4(1)
O1–P1–C19	91.2(2)	91.3(1)	94.4(5)	94.5(1)
C1–P1–C10	116.7(2)	116.4(1)	111.8(4)	131.0(2)
C1–P1–C19	118.0(2)	117.0(2)	118.4(5)	118.0(2)
C10–P1–C19	124.8(2)	126.0(2)	129.7(5)	110.9(2)
P1–C10–C15	133.5(3)	132.7(2)	134.6(7)	127.6(3)

Solvent Dependence of the Composition of 10$_{intra}$ and 10$_{inter}$

Since the X-ray structure of **10c** revealed the presence of unsolvated and solvated forms, the solvent influence upon the composition of **10** was examined (Table 2). In nondonor solvents, both **10a** and **10b** show the presence of only the intramolecular hydrogen-bonded species **10$_{intra}$**. Dissolution of **10a** in donor solvents, however, resulted in the facile formation of spirophosphorane **5a** even at room temperature, and a small upfield signal due to **10a$_{inter}$** could be observed along with that of **10a$_{intra}$**. Phosphorane **10b** also shows the presence of both forms and is less susceptible towards cyclization. As expected, **10c** shows different behavior, with the intermolecular hydrogen-bonded species **10c$_{inter}$** being the only observable species in donor solvents. When **10c$_{inter}$** containing a solvent molecule of EtOH was dissolved in nondonor solvents, a mixture of **10c$_{intra}$** and **10c$_{inter}$** was observed. The presence of **10c$_{inter}$** in nondonor solvents is a consequence of either interaction with EtOH or adventitious H_2O. These results indicate that for **10c**, compared with **10a** and **10b**, intramolecular hydrogen bonding is less favorable: the appearance of the intermolecular hydrogen-bonded species is instantaneous for **10a** and **10b** upon dissolution in donor solvents, whereas equilibration between the two forms of **10c** can be observed by NMR spectroscopy.

Table 2. ^{31}P NMR chemical shifts [ppm] of phosphoranes **10a**–**c** in various solvents.[a]

Solvent	10a		10b		10c (with EtOH)	
	intra	inter	intra	inter	intra	inter
Hexane	–53.0[b]		–35.5		–15.5	–43.9
Benzene	–52.6[b]		–34.2		–14.5	–42.8
Chloroform	–51.9[b]		–34.4		–14.7	–43.0
Diethyl ether	–53.4[b]		–35.0	–52.3		–42.2
Acetone		–68.8[b]		–51.4		–40.1
Tetrahydrofuran		–70.6[b]		–53.0		–41.2
Acetonitrile		[c]		–51.4		–39.7
Methanol		[c]		–52.3		–40.6
Pyridine		[c]		–53.2		–39.3

[a] "intra" refers to the intramolecular hydrogen-bonding species, and "inter" to the intermolecular hydrogen-bonding species. [b] The signal of the cyclized compound **5a** or **5b** was also observed. [c] Only the signal of **5a** was observed.

Ligand Exchange of the P–H$_{apical}$ Phosphoranes 10

The dynamic behavior of **10b** (R = *n*Bu), whose ^{19}F signals could be assigned as shown in Figure 3 by signal broadening due to through-space coupling[25] between *a-endo* and *b-endo*, and by ^{19}F NMR irradiation experiments, was examined by variable-temperature ^{19}F NMR measurements. No evaluation of **10a** (R = Me) could be carried out because of its labile nature.

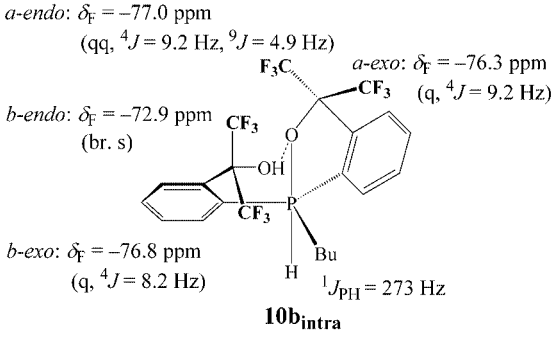

Figure 3. ^{19}F NMR assignment of **10b**.

Ordinary pseudorotation involving interconversion between *P*-enantiomers should result in coalescence between the signals corresponding to *a-endo* and *a-exo*, and between those of *b-exo* and *b-endo*. However, what was actually observed was the coalescence between signals corresponding to *a-exo* and *b-exo*. Thus, other than the pseudorotation between *P*-enantiomers, the presence of a low-energy process was revealed, which interconverts the bidentate and the monodentate Martin ligand by a hydrogen shift. The barrier of this dynamic process was estimated to be $\Delta G^{\neq}$ = 17.7 kcal mol^{-1} ($\Delta\nu$ = 106 Hz) at 368 K in [D_8]toluene and $\Delta G^{\neq}$ = 17.4 kcal mol^{-1} ($\Delta\nu$ = 105 Hz) at 363 K in 1,2-dichlorobenzene, based upon the Gutowsky–Holm approximation.[26] A line-shape analysis of spectra taken in [D_8]-toluene gives an estimate of $\Delta H^{\neq}$ = 11.4 ± 1.7 kcal mol^{-1} and $\Delta S^{\neq}$ = –16.3 ± 4.7 eu.

Two mechanisms are plausible to account for the observed ligand-exchange reaction, one which involves a ring-opened 8-P-3 phosphane (**12**: path A) and one which involves a 12-P-6 transition state (**TS-i**: path B), where concomitant P–O bond formation and bond breaking is ac-

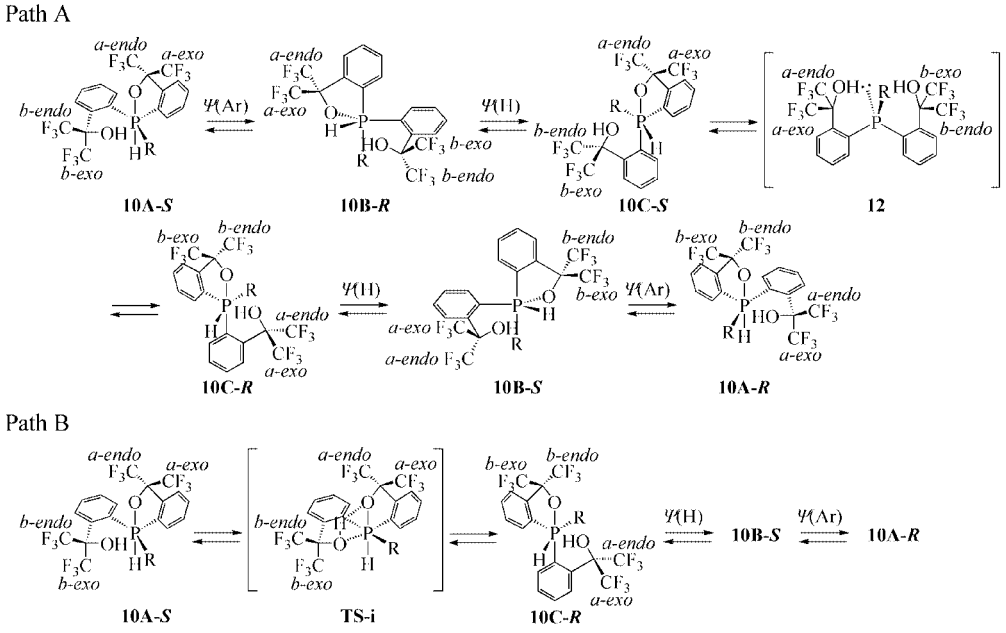

Scheme 3.

companied by a hydrogen shift from oxygen atom to oxygen atom, as shown in Scheme 3. The former path involves two pseudorotations and a ring opening to form the symmetric intermediate **12** and the same three processes to reach the enantiomer. The other mechanism involves direct transformation from **10A** to **10C**, as depicted in path B, followed by two low-energy pseudorotation processes to give the enantiomeric **10A**.

Since phosphoranes bearing a P–H bond are usually found in equilibrium with prototropic ring-opened isomeric phosphanes such as **12**, path A was initially thought more feasible. However, when **10b** was dissolved in MeOD and the NMR spectrum of the solution measured immediately, the O–H hydrogen atom was found to be completely exchanged with deuterium, whereas the P–H hydrogen atom was only partially exchanged. Since the ligand-exchange reaction is an extremely rapid process, if path A were operative the P–H hydrogen atom should also have been completely replaced by a deuterium atom due to the symmetric nature of intermediate **12**. However, since this is not the case, we believe that path B, which does not involve dissociation of the P–H bond, is more likely. Furthermore, dissolution of **10a**–**c** in ethereal solutions containing KOH led to complete conversion to species which we believe to be hexacoordinate [from **10a**: δ_P (Et_2O) = –153 ppm ($^1J_{P,H}$ = 679 Hz); from **10b**: δ_P (Et_2O) = –130 ppm ($^1J_{P,H}$ = 674 Hz); from **10c**: δ_P (Et_2O) = –117 ppm ($^1J_{P,H}$ = 335 Hz)] judging from the high-field ^{31}P chemical shifts. The $^1J_{P,H}$ values for **10a**,**b** are in good agreement with the reported values for hexacoordinate **13** (R = Me, $^1J_{P,H}$ = 620 Hz; R = Ph, $^1J_{P,H}$ = 642 Hz). This implies that attaining the hexacoordinate state is facile and therefore our assumption of a transition state such as **TS-i** is quite reasonable. Since the overall barrier for the exchange process is essentially the same in toluene (E_T^N = 0.099) and 1,2-dichlorobenzene (E_T^N = 0.225), it may well be that the global energy maximum (transition state) of the whole process (path B) is one of the pseudorotation transition states [Ψ(H) or Ψ(Ar)] and not **TS-i**.

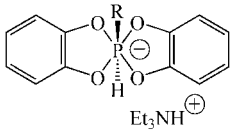

13 (R = Me, Ph)

Formation of *O-cis* Phosphoranes

While we were carrying out recrystallization of P–H phosphorane **10b** in MeCN at ambient temperatures, we obtained a crystalline compound **6b** that was neither **10b** nor **5b**.[18a] This same compound was also found to form along with **5b** when **10b** was heated in pyridine at ca. 60 °C and it gradually underwent conversion into **5b**. X-ray structural analysis (vide infra) of this compound revealed that it is an unexpected stereoisomer of **5b** bearing a carbon atom and an oxygen atom in a *trans* relationship in the apical positions, i.e., an *O-cis* relationship. Optimization of the reaction conditions to furnish *O-cis* **6b** led to a yield of 71% along with 29% of *O-trans* **5b**, as shown in Scheme 4, upon heating of **10b** in a THF/pyridine (5:1) mixture at 60 °C for 20 min. Phosphorane *O-cis* **6a** could also be obtained in 52% yield, along with 46% of *O-trans* **5a**, upon heating of a THF solution of **10a** at 40 °C for 1 h. However, the pseudorotation of *O-cis* **6a** to *O-trans* **5a** was found to take place gradually even at room temperature. In the case of **10c**, *O-cis* **6c** could be obtained in 75% yield along with 18% recovery of **10c** by refluxing in THF/pyridine (5:1) for 36 h.

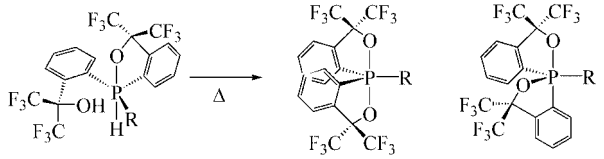

10a (R = Me) THF, 40 °C **5a**: 46% **6a**: 52%
10b (R = *n*Bu) THF/pyridine, 60 °C **5b**: 29% **6b**: 71%
10c (R = *t*Bu) THF/pyridine, reflux **5c**: – **6c**: 75%

Scheme 4.

X-ray Structure of the *O-cis* Phosphoranes

Figure 4 shows an ORTEP drawing of **6b** along with **5b** for comparison. Compound **6c** was also confirmed to have an *O-cis* structure. Selected structural parameters are listed in Table 3. Although the O1–P1–C10 angles for *O-cis* **6b** and **6c** are 170.5 and 169.5°, respectively, and deviate from the ideal value of 180°, the sums of the angles O2–P1–C1, C1–P1–C19, and C19–P1–O2 for *O-cis* **6b** and **6c** are 358.7, and 358.8°, respectively, and near the ideal value of 360°, thus indicating that the two compounds indeed take on trigonal-bipyramidal (TBP) structures, although they are somewhat distorted. The two figures clearly show that the two compounds are in a stereoisomeric relationship. The apical bond in *O-trans* **5b** was found to be less distorted, with an angle of 175.75°. A similar trend has been predicted in theoretical calculations on PH_3F_2, with the F_{apical},F_{apical} isomer having an F–P–F angle of 180° and the F_{apical}, $F_{equatorial}$ isomer (calculated with C_s symmetry) an apical bond angle of 171.6°.[9a] This propensity has also been predicted with the F_{apical},$F_{equatorial}$ isomer of $[SiH_3F_2]^-$ (175.5°).[27] On the other hand, the corresponding bonds in *O-cis* **6b** were found to be different, as expected, with the apical bonds being typically longer than the corresponding equatorial bonds (P–O_{apical} 1.773 > P–$O_{equatorial}$ 1.658 Å and P–C_{apical} 1.860 > P–$C_{equatorial}$ 1.806 Å). The percentages of contraction of an equatorial bond compared to that of an apical bond for **6b** are 6% for P–O and 3% for P–C, and are in good agreement with averaged (among three conformers) differences between P–O (4%) and P–H (2%) bonds in $PH_3(OH)_{apical}(OH)_{equatorial}$ by theoretical calculations,[12] thus reflecting the larger polarity of the P–O bond compared with the P–C bond. The trends are practically the same in *O-cis* **6c**.

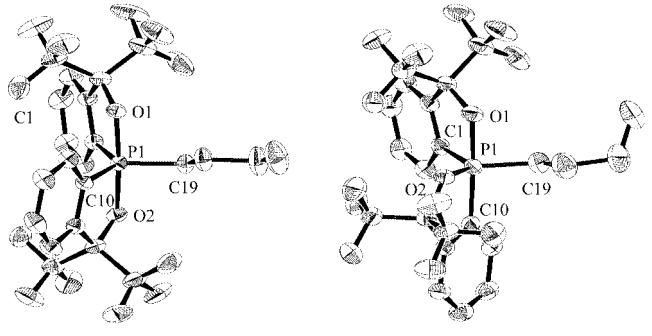

5b **6b**

Figure 4. ORTEP drawings of **5b** and **6b** showing the thermal ellipsoids at the 30% probability level. All the hydrogen atoms have been omitted for clarity.

Table 3. Selected bond lengths [Å] and angles [°] for **5b**, **6b**, and **6c**.

	5b[a]	**6b**[a]	**6c**[b]
P1–O1	1.765(2)	1.773(3)	1.771(3)
P1–O2	1.750(2)	1.658(3)	1.652(2)
P1–C1	1.822(2)	1.806(4)	1.830(4)
P1–C10	1.817(2)	1.860(4)	1.893(4)
P1–C19	1.818(3)	1.830(5)	1.875(4)
O1–P1–O2	175.75(8)	82.9(1)	82.9(1)
O1–P1–C1	87.30(9)	87.0(2)	85.6(1)
O1–P1–C10	90.73(9)	170.5(2)	169.5(1)
O1–P1–C19	91.3(1)	89.0(2)	90.4(2)
O2–P1–C1	90.84(9)	119.9(2)	120.7(2)
O2–P1–C10	87.32(9)	87.8(1)	87.5(1)
O2–P1–C19	92.9(1)	124.2(2)	116.3(2)
C1–P1–C10	126.8(1)	99.1(2)	95.7(2)
C1–P1–C19	116.5(1)	114.6(2)	121.8(2)
C10–P1–C19	116.6(1)	94.9(2)	97.7(2)

[a] Ref.[19c] [b] The crystal was found to contain two independent molecules. Values of only one are given.

Solution Structure of *O-cis* Spirophosphoranes: Rapid Enantiomer Interconversion

As a consequence of a rapid, single-step pseudorotation process between enantiomers **6-*R*** and **6-*S***, with the R group as the pivot, averaged spectra are observed for **6a–c** at ambient temperature. A comparison of the NMR spectra of *O-trans* **5** and *O-cis* **6** showed that for all three pairs of isomeric phosphoranes the ^{31}P NMR shift is located at lower field for **6** by around 15 to 17 ppm [δ_P ($CDCl_3$) = –22.6 ppm for **5a** and –6.3 ppm for **6a**; –18.8 ppm for **5b** and –3.5 ppm for **6b**; –9.8 ppm for **5c** and 7.7 ppm for **6c**]. The $^1J_{C(aryl),P}$ coupling constants for **5a**, **5b**, and **5c** are 177, 160, and 160 Hz, respectively, whereas those for **6b** and **6c** are 88 and 77 Hz; that of **6a** is obscured. Since the $^1J_{C(alkyl),P}$ coupling constants are essentially the same for each pair (**5a**: 125 Hz, **6a**: 130 Hz; **5b**: 116 Hz, **6b**: 114 Hz; **5c**: 103 Hz, **6c**: 114 Hz), it follows that the solution structures of these compounds are all essentially the same, i.e., trigonal bipyramids. Square-pyramid (SP) type structures would be expected to give coupling constants of similar magnitude for both aryl groups because both would occupy basal sites, which is not the case here. Unfortunately, low-temperature (down to 203 K) ^{13}C NMR measurements only gave broadened spectra for the two inequivalent Martin ligand carbon atoms of *O-cis* **6b** and **6c**. Since the $^1J_{C(alkyl),P}$ values for *O-trans* **5b** and *O-cis* **6b** coincide the best (115 Hz), from analogy of $^1J_{C(aryl),P}$ = 160 Hz for *O-trans* **5b**, we can assume that the equatorial $^1J_{C(aryl),P}$ coupling constant for *O-cis* **6b** is also 160 Hz, therefore the axial $^1J_{C(aryl),P}$ coupling constant is calculated to be 16 Hz from the observed average value of 88 Hz (88 × 2 – 160). This value relationship (large coupling constant for P–$atom_{equatorial}$ and small coupling for P–$atom_{apical}$) parallels that for $^1J_{P,H}$ in the P–H phosphoranes **10** (H_{apical}:

273–293 Hz) and **7** ($H_{equatorial}$: 729 Hz) in Scheme 2 (vide supra).

In the ^{19}F NMR spectra the two signals observed at room temperature for *O-cis* **6b** [^{19}F NMR ($CDCl_3$, 293 K): δ = –74.9 (q, $^4J_{F,F}$ = 8.5 Hz, 6 F), –76.2 ppm (q, $^4J_{F,F}$ = 8.5 Hz, 6 F)] decoalesce into four signals [^{19}F NMR ([D_8]-toluene, 193 K): δ = –74.3 (br. s, 3 F), –74.5 (br. s, 3 F), –75.5 (br. s, 3 F), –76.0 ppm (br. s, 3 F)] at low temperatures. The fact that only one ^{31}P signal [^{31}P NMR ([D_8]-toluene, 219 K): δ = –3.6 ppm] is observed for the compound throughout the temperature range confirms that the ^{19}F NMR signals are for a single species. Coalescence lineshape analysis of the better resolved upper-field pair of signals gave estimated activation parameters for the process, i.e., interconversion by a single BPR, to be $\Delta H^{\neq}$ = 10.0 ± 0.7 kcal mol^{-1} and $\Delta S^{\neq}$ = –3.4 ± 3.0 eu.[26] The lower-field pair was broadened further at low temperature, presumably by the suppression of CF_3-group rotation. Decoalescence of signals for *O-cis* **6c** could not be observed even at 193 K ([D_8]toluene). This implies that the inversion barrier for *O-cis* **6c** is smaller than for *O-cis* **6b** due to the presence of the bulky *t*Bu group, which could distort the ground-state structure of *O-cis* **6c** somewhat towards the square-pyramidal transition state of pseudorotation (Scheme 5).

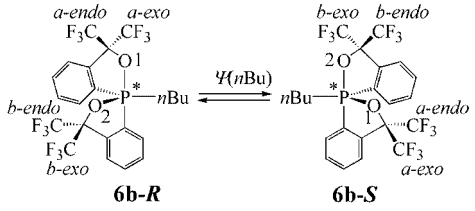

Scheme 5.

Cyclization of 10b to 5b in Nondonor Solvents

In order to gain insight into the mechanism of the cyclization reaction of **10b**, we carried out kinetic studies. This cyclization reaction is also interesting from the point of view that it can serve as a model for the heterolytic cleavage of element–hydrogen or element–carbon bonds to give compounds bearing new element–heteroatom bonds with concomitant elimination of H_2 or hydrocarbon. In the case of second-row elements and below, there have been suggestions that species of extra coordination are involved during the reaction.[28] We also have previously observed selective hydrocarbon elimination in the intramolecular cyclization reaction of acyclic 8-Si-4 *o*-silylbenzyl alcohols to 8-Si-4 cyclic alkoxysilanes via 10-Si-5 transition states,[29a] in the hydrolysis of monocyclic 12-Sb-6 ate complexes to monocyclic 10-Sb-5 stiboranes,[29b] and in the transformation of monocyclic 10-Bi-5 alcohols to 10-Bi-5 spirobismuthanes via 12-Bi-6 transition states.[29c] As for phosphorus, this phenomenon is not normally encountered with neutral compounds of ordinary valency. However, the facile hydrolysis of tetracoordinate phosphonium cations is known to proceed via pentacoordinate intermediates,[30] and the exchange reaction of alkoxy and amino groups of phosphites with other alcohols and amines has been determined to involve pentacoordinate P–H intermediates.[4,31] As for transformations involving hypervalent reactants and products, little has been reported as the lack of available thermodynamically stable compounds and their susceptibility to moisture has complicated kinetic examinations.[32]

The rates of cyclization of **10b** to yield **5b** were measured in [D_8]toluene (E_T^N = 0.099,[33] DN^N = 0.01[34]) and *o*-dichlorobenzene (E_T^N = 0.225,[33] DN^N = 0.08[34]), which can be considered to be nondonor solvents, in the temperature range 343–373 K by monitoring the change in the ^{19}F NMR integrals. All the measurements were found to obey first-order kinetics (Table 4). The activation parameters obtained are as follows: in toluene, $\Delta H^{\neq}$ = 17.3 ± 0.6 kcal mol^{-1} and $\Delta S^{\neq}$ = –34.7 ± 1.7 eu; in *o*-dichlorobenzene, $\Delta H^{\neq}$ = 14.3 ± 0.2 kcal mol^{-1} and $\Delta S^{\neq}$ = –41.0 ± 0.6 eu. Cyclization was found to be slightly faster in the more polar *o*-dichlorobenzene, and the negative activation entropy values were found to be quite large for both solvents, with that of *o*-dichlorobenzene being somewhat larger.

Cyclization of 10b to 5b and 6b in Pyridine

Cyclization in pyridine (308–323 K) was found to yield both *O-trans* **5b** and *O-cis* **6b**. Thus, the measurements were analyzed according to Equations (1), (2), and (3), with the rate constants corresponding to the reactions in Scheme 6, where [**5b**], [**6b**], and [**10b**] denote the concentration of **5b**, **6b**, and **10b** at arbitrary intervals; the subscript "0" denotes concentration at t = 0.

Table 4. The cyclization reactions of **10b** to **5b** in nondonor solvents.[a,b]

Solvent	Temp. [K]	Rate [s^{-1}]	$\Delta H^{\neq}$ [kcal mol^{-1}]	$\Delta S^{\neq}$ [eu]
Toluene	343	(1.76 ± 0.05) × 10^{-6}	17.3 ± 0.6	–34.7 ± 1.7
	353	(3.95 ± 0.08) × 10^{-6}		
	363	(8.15 ± 0.12) × 10^{-6}		
	373	(1.46 ± 0.12) × 10^{-5}		
o-Dichlorobenzene	343	(9.87 ± 0.23) × 10^{-6}	14.3 ± 0.2	–41.0 ± 0.6
	353	(1.84 ± 0.07) × 10^{-5}		
	363	(3.32 ± 0.02) × 10^{-5}		
	373	(5.55 ± 0.05) × 10^{-5}		

[a] The process was monitored by ^{19}F NMR spectroscopy. [b] Error is given as standard deviation.

$$[\mathbf{10b}] = [\mathbf{10b}]_0\exp\{-(k_1 + k_3)t\} \quad (1)$$

$$[\mathbf{6b}] = [\mathbf{10b}]_0\{k_1/(k_2 - k_1 - k_3)\}[\exp\{-(k_1 + k_3)t\} - \exp(-k_2)t] \quad (2)$$

$$[\mathbf{5b}] = [\mathbf{10b}]_0[1 - \{(k_2 - k_3)/(k_2 - k_1 - k_3)\}\exp\{-(k_1 + k_3)t\} + k_1/(k_2 - k_1 - k_3)\exp(-k_2)t] \quad (3)$$

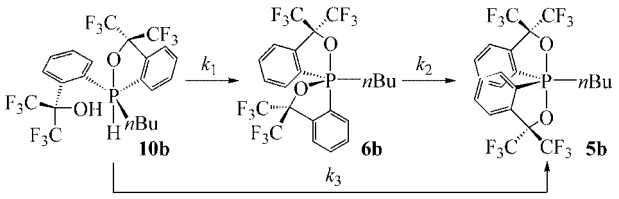

Scheme 6.

Figure 5, Table 5, and Figure 6 show examples of the curve fitting of the measurements at 323 K, each depicting the observed relative concentrations of **10b**, **6b**, and **5b**, the calculated rates, and the Eyring plot of these rates. Compared with the cyclization in nondonor solvents, the rates for the formation of both *O-trans* **5b** and *O-cis* **6b** are much larger, whereas the pseudorotation rates stay essentially the same (vide infra). The data indicate that the path for direct *O-trans* **5b** formation (k_3) is entropy-favored and that for *O-cis* **6b** is enthalpy-driven (k_1). The fact that the pseudorotation of *O-cis* **6b** to *O-trans* **5b** (k_2) is 4–5-fold slower than the formation of both *O-trans* **5b** and *O-cis* **6b** from **10b** is noteworthy.

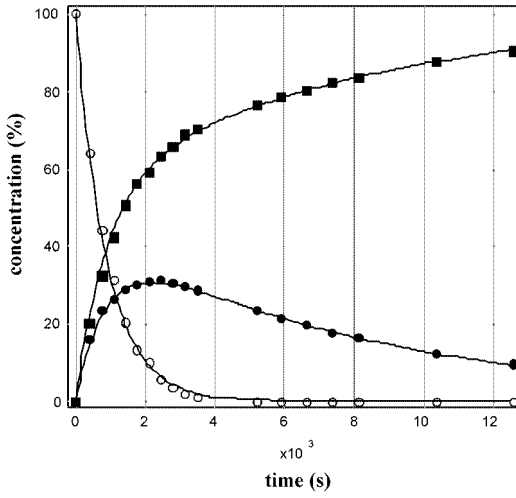

Figure 5. Rate profile showing the relative concentrations of **10b** (open circles), **5b** (filled circles), and **6b** (filled squares) for the thermal reaction of **10b** in pyridine at 323 K.

Table 5. The cyclization reactions of **10b** in pyridine.[a,b]

Process	Temp. [K]	Rate [s^{-1}]	$\Delta H^{\neq}$ [kcal mol^{-1}]	$\Delta S^{\neq}$ [eu]
k_1	308	$(1.17 \pm 0.07) \times 10^{-4}$	17.1 ± 0.3	–21.0 ± 1.1
(**10b** → **6b**)	313	$(1.83 \pm 0.05) \times 10^{-4}$		
	318	$(2.82 \pm 0.26) \times 10^{-4}$		
	323	$(4.52 \pm 0.20) \times 10^{-4}$		
k_2	308	$(2.63 \pm 0.08) \times 10^{-5}$	20.3 ± 0.5	–13.8 ± 1.7
(**6b** → **5b**)	313	$(4.36 \pm 0.11) \times 10^{-5}$		
	318	$(7.83 \pm 0.38) \times 10^{-5}$		
	323	$(1.26 \pm 0.04) \times 10^{-4}$		
k_3	308	$(1.04 \pm 0.14) \times 10^{-4}$	23.9 ± 1.3	+0.8 ± 4.2
(**10b** → **5b**)	313	$(1.74 \pm 0.09) \times 10^{-4}$		
	318	$(3.33 \pm 0.41) \times 10^{-4}$		
	323	$(6.64 \pm 0.43) \times 10^{-4}$		

[a] The process was monitored by ^{19}F NMR spectroscopy. [b] Error is given as standard deviation.

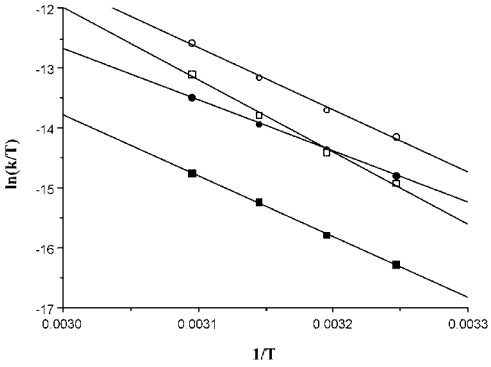

Figure 6. Eyring plot of the rates $k_1 + k_3$ (open circles), k_1 (open squares), k_2 (filled squares), and k_3 (filled circles) calculated from curve fitting of the rate profiles of the thermal reaction of **10b** in pyridine (Scheme 6).

Cyclization of 10c to 5c and 7

The cyclization reaction of **10c** was carried out after removal of the solvent molecule in vacuo. The rates were found to be very slow, as a whole, compared with those of **10b** (Scheme 7, Table 6). *p*-Xylene (E_T^N = 0.074, DN^N = 0.13) and *o*-dichlorobenzene were used as nondonor solvents in the temperature range 393–423 K. Because of the complexity of the ^{19}F NMR spectra of **10c**, the ^{31}P NMR spectrum was monitored instead. We found that both *O-trans* **5c** and **7** were formed, the latter as a consequence of the loss of the *tert*-butyl group. In the case of *p*-xylene as solvent, whereas an appreciable amount of **7** was observed at 393 K, only trace amounts were detected at higher temperatures. The rate of formation of **7** was considerably higher in *o*-dichlorobenzene than in *p*-xylene. The absolute values of the activation entropies for the formation of *O-trans* **5c** were found to be quite small compared with those of *O-trans* **5b** formation. In *o*-dichlorobenzene, for instance, the value for *O-trans* **5b** is –41 eu whereas it is –10 eu for *O-trans* **5c**. The activation entropy for the formation of **7** was found to have a larger negative value (–22 eu) than that of the *O-trans* **5c** forming process (–10 eu).

The effect of using pyridine as solvent was dramatic. Only the less stable rotamer *O-cis* **6c** was formed at temperatures considerably lower than those required for the formation of *O-trans* **5c** in nondonor solvents. In this case it should also be noted that the cyclization of **10b** to *O-cis* **6c** is significantly faster than the pseudorotation of *O-cis* **6c** to *O-trans* **5c**.

Table 6. The cyclization reactions of **10c** in various solvents.[a]

Solvent	Product	Temp. [K]	Rate [s^{-1}]	$\Delta H^{\neq}$ [kcal mol^{-1}]	$\Delta S^{\neq}$ [eu]
p-Xylene[b]	**5c**	393	$(1.14 \pm 0.02) \times 10^{-6}$	32.2 ± 1.1	–4.2 ± 2.6
		403	$(3.66 \pm 0.07) \times 10^{-6}$		
		413	$(9.58 \pm 0.10) \times 10^{-5}$		
		423	$(1.46 \pm 0.04) \times 10^{-5}$		
	7	393	$(3.15 \pm 0.20) \times 10^{-7}$		
o-Dichlorobenzene[b]	**5c**	393	$(2.06 \pm 0.01) \times 10^{-6}$	29.5 ± 0.7	–9.9 ± 1.8
		403	$(5.73 \pm 0.10) \times 10^{-6}$		
		413	$(1.45 \pm 0.04) \times 10^{-5}$		
		423	$(3.22 \pm 0.07) \times 10^{-5}$		
	7	393	$(1.81 \pm 0.02) \times 10^{-6}$	25.0 ± 1.0	–21.8 ± 2.6
		403	$(3.84 \pm 0.08) \times 10^{-6}$		
		413	$(8.06 \pm 0.09) \times 10^{-6}$		
		423	$(1.92 \pm 0.03) \times 10^{-5}$		
Pyridine[c]	**6c**	333	$(2.75 \pm 0.03) \times 10^{-5}$	22.3 ± 0.6	–12.7 ± 1.8
		343	$(8.43 \pm 0.11) \times 10^{-5}$		
		353	$(2.04 \pm 0.03) \times 10^{-4}$		
		363	$(4.93 \pm 0.08) \times 10^{-4}$		

[a] Error is given as standard deviation. [b] The process was monitored by ^{31}P NMR spectroscopy. [c] The process was monitored by ^{19}F NMR spectroscopy.

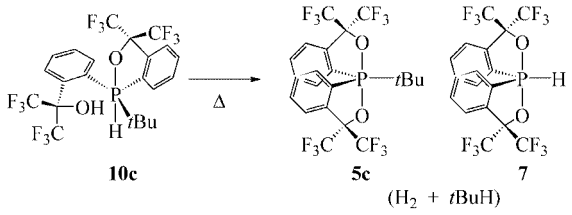

Scheme 7.

Mechanism of the Cyclization Reaction

If we assume that nucleophilic reaction to a pentacoordinate phosphorus atom occurs with equatorial edge attack, as is generally accepted,[35] then rationalization of the mechanism for formation of the *O-cis* isomer in a donor solvent (pyridine) becomes straightforward by considering configuration **10A** as the reacting species, where P–H is apical and P–C(aryl) is equatorial (Scheme 8).[36] Attack of the hydroxy oxygen atom from the rear side of the P–C(aryl) bond to form a pseudohexacoordinate phosphorus species with concomitant H_2 extrusion and pyridine dissociation by a four-membered concerted reaction, as depicted in **TS-*cis***, would give *O-cis* **6** with the newly formed P–O bond becoming the new apical bond (P–O1). This mechanistic rationale is appropriate for the following four reasons. First of all, since P–H phosphoranes **10** have only one P–O bond, whereas spirophosphoranes *O-trans* **5** and *O-cis* **6** have two, it is reasonable to assume that the latter are more stable as hypervalent species. Thus, it is reasonable to assume that the transition state of the cyclization reaction is reactant-like (**TS-*cis***) and TBP features of the reactant are retained to a large extent. Secondly, the reactant takes on its lowest energy configuration with **10A** and thus the formation of *O-cis* **6** requires only a minimal amount of motion. Thirdly, attack of the oxygen atom to the σ*-orbital of the P–C(aryl) bond to form the new apical P–O1 bond is expected to be energetically more favorable than attack to the σ*-orbital of the P–C(alkyl) bond, which would lead to the formation of the $O_{equatorial}$,$O_{equatorial}$ isomer. This rotamer would easily give the *O-trans* isomer **5** upon a single pseudorotation. Last of all, having the H atom already apical is not only favorable in terms of apicophilicity but also due to the fact that it is weakly bonded to the phosphorus atom in TBP structures, thus enabling facile bond dissociation en route to products via a four-membered cyclic transition state. Although an ionic stepwise mechanism cannot be fully excluded, we believe it is not likely because a stable anionic hexacoordinate species would have to be regarded as the reactive species, and this conflicts with the fact that monodeprotonation of **10a** (Me) with aqueous KOH in Et_2O results in the facile formation of a stable hexacoordinate species [^{31}P NMR: δ = –153 ppm ($^1J_{P,H}$ = 679 Hz)] that is much less prone to cyclization than **10a** itself.

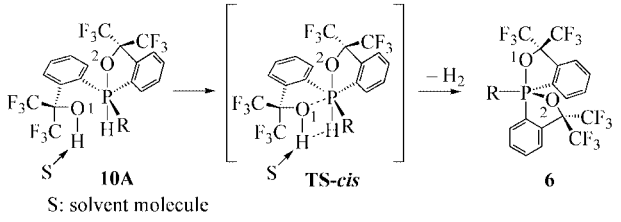

Scheme 8.

As for the formation of *O-trans* **5b** (*n*Bu) in donor solvents, the fact that the rate of formation of *O-trans* **5b** is similar to that of *O-cis* **6b** (Table 5) makes *O-trans* **5b** formation by unfavorable oxygen attack the σ*-orbital of the P–C(alkyl) bond in configuration **10A** highly unlikely (Scheme 9). Also, a rather large negative value for the activation entropy would have been expected because a more progressed and thus tighter transition state would be necessary. It follows that the formation of *O-trans* **5b** requires pseudorotation to a different configuration (such as intermediate **10F**), where P–H is apical and P–O is equatorial, and which is inevitably higher in energy than **10A**, to precede the cyclization (**TS-*trans***). Thus, the enthalpy value of

23.9 kcal mol^{-1} (considerably larger than the value of 17.1 kcal mol^{-1} for the path that gives *O-cis* **6b**: **TS-*cis***) could be considered the result of a combination of two barriers, that of pseudorotation and cyclization. Pseudorotation would allow **10b** to take on configurations in which the oxygen atom could attack the electronically favorable σ*-orbital of a P–O bond. Considering the fact that the apicophilicity order is H > aryl > alkyl and that it is the hydrogen atom on the phosphorus atom that is removed from the molecule, configuration **10F** can be considered to be the reactive intermediate. This species can be generated by a three-step pseudorotation process without passing through high-energy species, with the bidentate ligand occupying diequatorial positions. The transition state is probably also concerted in this case, with concomitant pyridine dissociation (vide supra). The fact that the activation entropy for formation of *O-cis* **6b** is more negative than for *O-trans* **5b** formation may be due to a somewhat later transition state and thus more progressive bond formation for the former process. That *O-trans* **5c** (*t*Bu) could not be observed in the cyclization of **10c** in pyridine (Table 6) probably reflects the fact that the pseudorotation barrier for **10c** is much higher than that for **10b** from a steric point of view, since the required passage through **10E**, which bears an apical *t*Bu group, is thermodynamically quite unfavorable.

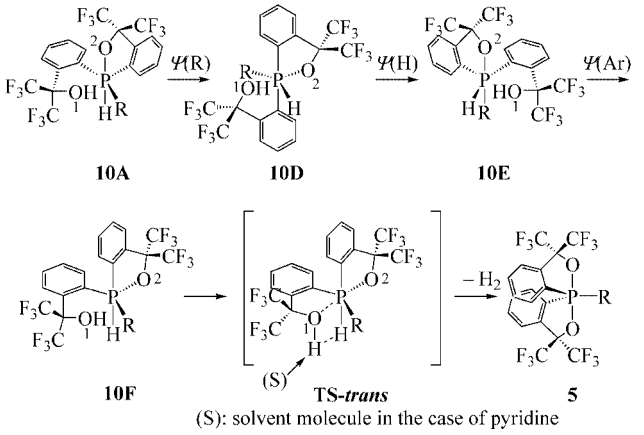

Scheme 9.

The mechanism for the formation of the stable *O-trans* isomer **5** in nondonor solvents is less obvious, since the temperatures required for the cyclization to *O-trans* **5b** (*n*Bu; Table 4) exceed those required for pseudorotation of *O-cis* **6b** to *O-trans* **5b** (Table 5). It is possible that the initial product is unobserved *O-cis* **6**, which quickly pseudorotates to *O-trans* **5** under the reaction conditions, or that **10F** (Scheme 9) is the reactive species as in the donor solvent case and directly gives rise to *O-trans* **5c**. In the case of **10c** (*t*Bu), the rate of formation of *O-trans* **5c** was found to be only slightly slower than the pseudorotation of *O-cis* **6c** to *O-trans* **5c** (Table 6), the latter of which is expected to be essentially independent of the solvent. Thus, if *O-trans* **5c** were to form by a sequence of *O-cis* **6c** formation followed by pseudorotation, then the latter transformation would be expected to be observed during the cyclization reactions in nondonor solvents. However, this was not the case. Therefore, for **10c** it is highly likely that the cyclization in nondonor solvents gives *O-trans* **5c** directly via **10F**. By analogy, we expect the cyclization of **10b** to be the same. For the cyclization of **10b** in nondonor solvents, the fact that $\Delta S^{\neq}$ has a large negative value and that $\Delta H^{\neq}$ decreases in the more polar *o*-dichlorobenzene ($k_{o\text{-dichlorobenzene}}/k_{toluene}$ = 3.8–5.6) is consistent with a concerted mechanism, as proposed for the reaction in pyridine, that differs only in the absence of an interacting solvent molecule. The solvent effect for **10c** ($k_{o\text{-dichlorobenzene}}/k_{p\text{-xylene}}$ = 1.8–2.2) is similar. Concerted reactions such as sigmatropic reactions are known to exhibit only small solvent effects in such a case as this.[37]

Both **TS-*cis*** (Scheme 8) and **TS-*trans*** (Scheme 9) are expected to be lowered in energy in pyridine due to the increased nucleophilicity of the hydroxy oxygen atom. However, since the activation energy for **TS-*trans*** is a combination of pseudorotation (not affected by solvent) and a ring-

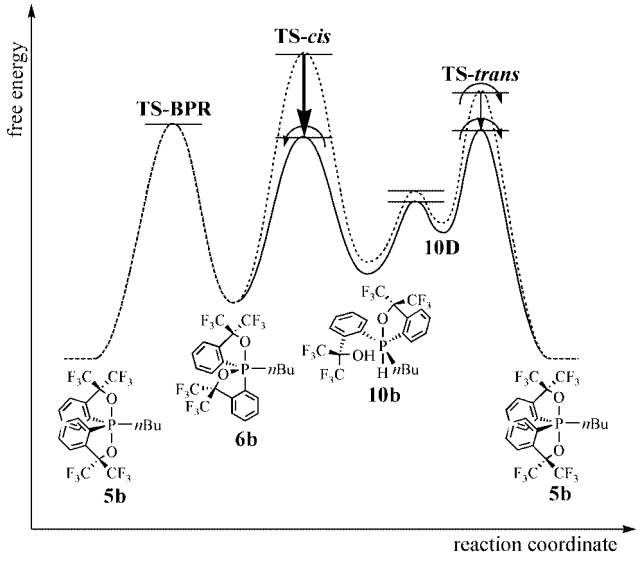

Figure 7. Energy profile for the thermal reaction of **10b**. The broken line and bold line correspond to reactions in nondonor solvents and in pyridine, respectively. The curved arrows denote the observed pathways for each group of solvents. The straight arrows show the degree of stabilization upon changing the solvent.

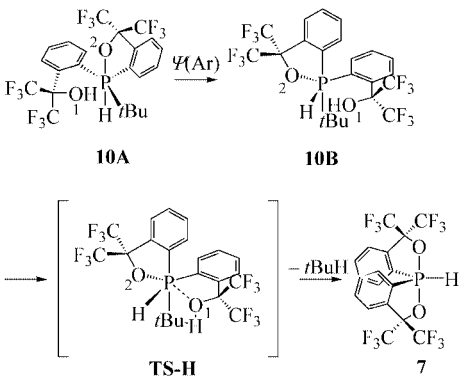

Scheme 10.

closure processes, the relative degree of stabilization should be less for **TS-*trans***, as is observed (Figure 7).

Reasoning analogous to that for the direct formation of **5** can be applied to the formation of **7**, as depicted in Scheme 10. X-ray structures show that, compared with **10b** (*n*Bu; 1.812 Å), there is a notable increase in the P–C(alkyl) bond length in $\mathbf{10c_{intra}}$ (*t*Bu; 1.854 Å) with still further elongation in $\mathbf{10c_{inter}}$ (*t*Bu; 1.878 Å), in which a P–O interaction is present (Figure 2), thus implying the potential for the P–*t*Bu bond to undergo cleavage.

Pseudorotation of the *O-cis* Isomer to the *O-trans* Isomer

The rates of pseudorotation of *O-cis* **6** to *O-trans* **5**, an apparently irreversible process, were measured by monitoring the ^{19}F NMR spectra in toluene (302–328 K; E_T^N = 0.099,[33] DN^N = 0.003,[34] β = 0.11[38]), pyridine (313–328 K; E_T^N = 0.302, DN^N = 0.85, β = 0.64), and ethanol (313–328 K; E_T^N = 0.654, DN^N = 0.82, β = 0.77) for *O-cis* **6b**, and in *p*-butyltoluene (expected to have physical properties similar to *p*-xylene) for *O-cis* **6c**. All the measurements conformed to first-order kinetics, and activation parameters could be estimated from the Eyring plot of the rates (Table 7, Figure 8). The rates for *O-cis* **6b** in pyridine were taken from the complex reaction of **10b** (Scheme 6). An independent measurement of isolated *O-cis* **6b** at 313 K (independent: 4.24×10^{-5} s^{-1}; curve fitting: 4.36×10^{-5} s^{-1}) confirmed the validity of the rates derived from the curve fitting (vide infra). For *O-cis* **6b**, the rates in pyridine and ethanol differ from that in toluene by less than 10% at the same temperatures [(1.26, 1.16, and 1.29)$\times10^{-4}$ s^{-1}, respectively, at 323 K]. Therefore, only a very small solvent effect is present and thus mechanisms involving proton-catalyzed P–O bond dissociation/recombination with intervention of highly polar species can be disregarded. The magnitude of the entropy is not so large and the sign is negative, as expected from the pseudorotation between previously examined diastereomeric *O-trans* spirophosphoranes.[8]

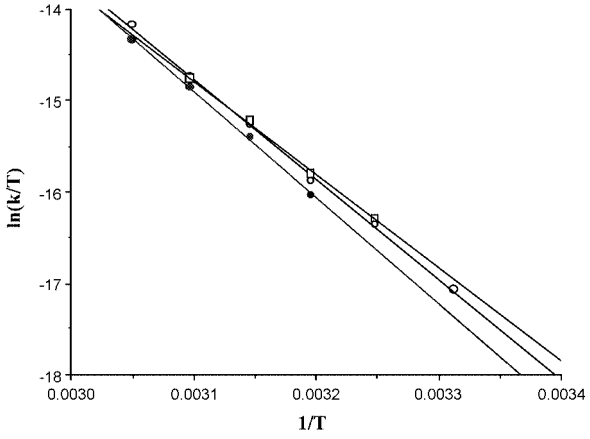

Figure 8. Eyring plot of the rates of stereomutation of **6b** to **5b** in toluene (open circles), pyridine (open squares), and ethanol (filled circles).

Relative Stability of the Stereoisomers *O-trans* 5 and *O-cis* 6

Here we take it for granted that the stereomutation of *O-trans* **5** [*21* (**5-*S***) or *12* (**5-*R***)] to its enantiomer (*12* or *21*) follows Berry pseudorotation. In principle, up to 20 stereoisomers are possible, as depicted in the Desargues–Levi diagram (Figure 9).[39] For the present group of isomeric spirophosphoranes, including *O-trans* **5** and *O-cis* **6**, a bidentate ligand cannot span between the two apical positions. Hence, the four stereoisomers *13*, *31*, *24*, and *42* can be eliminated as probable isomers. In the case where a five-membered bidentate ligand lies in the equatorial plane, the stereoisomers should be of high energy because of ring

Table 7. Rates and activation parameters of the stereomutation of *O-cis* **6** to *O-trans* **5**.[a,b]

	Solvent	Temp. [K]	Rate [s^{-1}]	$\Delta H^{\neq}$ [kcal mol^{-1}]	$\Delta S^{\neq}$ [eu]
6b	toluene	302	$(1.18\pm0.01)\times10^{-5}$	21.8 ± 0.4	–9.0 ± 1.2
		308	$(2.45\pm0.04)\times10^{-5}$		
		313	$(4.03\pm0.07)\times10^{-5}$		
		318	$(7.61\pm0.12)\times10^{-5}$		
		323	$(1.29\pm0.01)\times10^{-4}$		
		328	$(2.31\pm0.01)\times10^{-4}$		
	pyridine	308[c]	$(2.63\pm0.08)\times10^{-5}$	20.3 ± 0.5	–13.8 ± 1.7
		313[c]	$(4.36\pm0.11)\times10^{-5}$		
		313[d]	$(4.24\pm0.09)\times10^{-5}$		
		318[c]	$(7.83\pm0.38)\times10^{-5}$		
		323[c]	$(1.26\pm0.04)\times10^{-4}$		
	ethanol	313	$(3.44\pm0.03)\times10^{-5}$	23.1 ± 0.5	–5.3 ± 1.5
		318	$(6.56\pm0.05)\times10^{-5}$		
		323	$(1.16\pm0.03)\times10^{-4}$		
		328	$(1.97\pm0.02)\times10^{-4}$		
6c	*p*-butyltoluene	403	$(6.73\pm0.10)\times10^{-6}$	27.2 ± 0.8	–13.1 ± 1.8
		423	$(3.89\pm0.02)\times10^{-5}$		
		443	$(2.15\pm0.04)\times10^{-5}$		
		463	$(7.62\pm0.02)\times10^{-5}$		

[a] The process was monitored by ^{19}F NMR spectroscopy. [b] Error is given as standard deviation. [c] Values from the cyclization reaction of **10b** in pyridine. [d] Measured with isolated **6b** and not included in the activation parameter calculations.

strain. Among these isomers, *35*, *53*, *45*, and *54* can be considered to be higher in energy than *15*, *51*, *25*, and *52* because isomers of the former group bear two apical carbon substituents. Thus, since the BPR process requires passage through at least one of these groups of isomers, it is more appropriate to assume the latter. The isomers next highest in energy are *34* and *43*, which have two oxygen substituents in the equatorial plane but do not possess an equatorial bidentate ligand. That leaves *23*, *41*, *32*, and *14* (*O-cis* **6**) and the most stable isomers *12* and *21* (*O-trans* **5**). Because of the symmetry of the molecules, the pairs (*15*, *52*), (*25*, *51*), (*23*, *14*), (*41*, *32*), (*54*, *35*), and (*53*, *45*) are degenerate. Hence, the pathway for the interconversion between enantiomers of the most stable isomers *12* and *21* is reduced to *12–43–25–41–23–15–34–21* (shown as bold lines) or *12–43–51–32–14–52–34–21* (shown as a combination of bold and normal lines), which are degenerate. Here the process *41–23* (or *32–14*) corresponds to interconversion of enantiomers of *O-cis* **6**. Therefore, it follows that the interconversion between enantiomers of *O-trans* **5** (*12* and *21*) and transformation of *O-cis* **6** to *O-trans* **5** (*23* or *41* to *21* or *12*) involve a common pathway and thus the same global transition state, whether the actual transition state be of TBP structure or of SP structure, or whether the whole conversion process involves seven or five steps. Thus, the difference in activation energy between the interconversion and the transformation processes would, in principle, give the energy difference between isomers *O-trans* **5** and *O-cis* **6** directly. The activation parameters for the transformation of *O-cis* **6b** to *O-trans* **5b** were obtained as $\Delta H^{\neq}$ = 21.8 kcal mol^{-1} and $\Delta S^{\neq}$ = –9.0 eu (Table 7). Unfortunately, however, the interconversion barrier between enantiomers of *O-trans* **5** was too high to be measured by methods that allow the use of symmetric compounds.[17d] Thus, we resorted to comparing with compounds **14b-*endo*** and **14b-*exo***, which differ from *O-trans* **5** in only having one CH_3 group in place of one of the four CF_3 groups. The averaged activation parameters were $\Delta H^{\neq}$ = 33.7 kcal mol^{-1} and $\Delta S^{\neq}$ = –8.0 eu for the interconversion of the pair of **14**.[8] Thus, *O-cis* **6b** should be less stable than *O-trans* **5b** by about 12 (33.7 – 21.8) kcal mol^{-1}. Since the oxygen atom in the Martin ligand is expected to be slightly more apicophilic than the oxygen atom attached to the asymmetric carbon atom in **14**, the actual difference should be somewhat larger. At first glance, this difference of 12 kcal mol^{-1} would seem rather large for a compatible pair of stereoisomers, although they are only compatible because of the pseudorotation barrier that separates them. However, this value is in good agreement with theoretical calculations on the Me pair of *O-trans* **5a** and *O-cis* **6a**, which have a difference of 14.1 kcal mol^{-1}.[19c] The use of the difference in activation entropy of the Me pair to account for that of the *n*Bu pair of *O-trans* **5b** and *O-cis* **6b** is justified because a kinetic examination on the pseudorotation of a diastereomeric pair

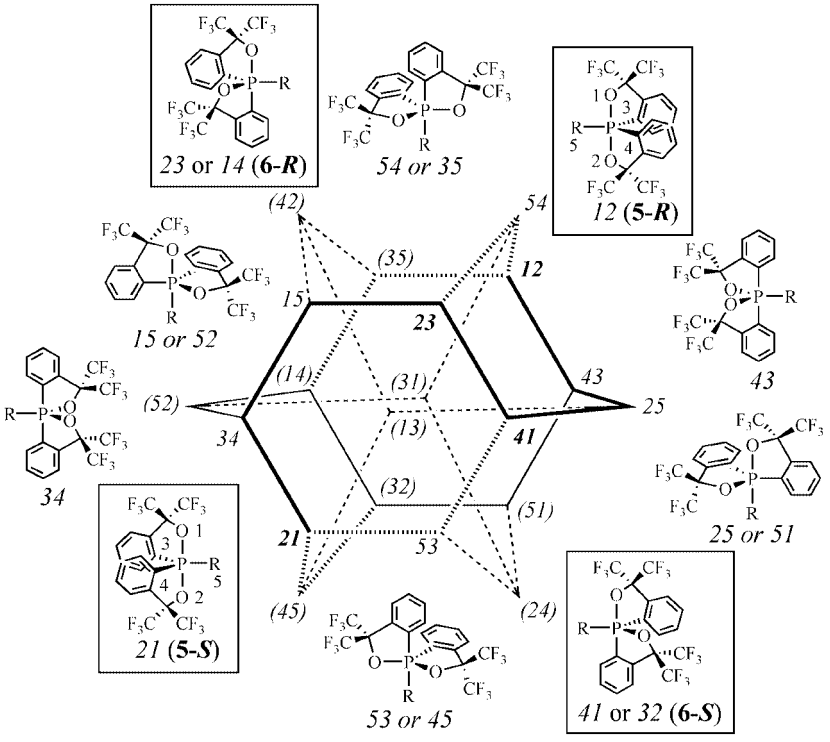

Figure 9. Simplified Desargues–Levi diagram for the pseudorotation of spirophosphoranes **5** and **6**. The two-digit numerals correspond to the substituents occupying the apical positions. Substituent priority numbers were arbitrarily assigned as shown for configurations *21* and *12*. The pathways to consider are shown as bold lines. Paths involving vertices corresponding to *13*, *31*, *24*, and *42*, which are not probable due to the ring effect, and those involving superficially identical compounds due to degeneracy (C_2 symmetry of the compounds), are shown as dotted and normal lines, respectively.

of **14a** bearing an equatorial methyl group in the place of an equatorial *n*Bu group in **14b** shows that the primary difference in the rate of interconversion between the equatorial Me and *n*Bu series (**14a**: $\Delta G^{\neq}$ = 34.7 kcal mol^{-1}; **14b**: $\Delta G^{\neq}$ = 36.3 kcal mol^{-1}) is entropy, and that the enthalpy of activation is essentially the same (**14a**: $\Delta H^{\neq}$ = 33.5 kcal mol^{-1}; **14b**: $\Delta H^{\neq}$ = 33.7 kcal mol^{-1}).[8] The Berry pseudorotation pathway of lowest energy for the inversion of *O-trans* **5** should be the path shown in Figure 9, considering the comprehensive analysis carried out by Holmes.[10,40]

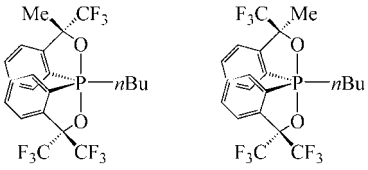

14b-*endo* **14b-*exo***

There still remains the question of whether the diequatorial oxygen isomers (*34* and *43*), the species attained by a single pseudorotation of **5b** with the *n*Bu group as the pivot, actually exists as an energy-minimum species. As we can make a tentative guess from the kinetic parameters deduced from these studies for our system, intermediate **A** (**A-*R*** or **A-*S*** in Figure 10), were it to exist, is expected to be energetically less stable than **6b** from usual apicophilicity considerations, and thus the energy difference should be more (probably by at least a few kcal mol^{-1}) than the value of 12 kcal mol^{-1} given above for the difference between **5b** and **6b**. As for the activation energy for the one-step pseudorotation process between **5b** and **A**, it can be estimated to be roughly the same (10 kcal mol^{-1}) as that for the process between enantiomers of **6b** because both pseudorotations involve a single step with the same pivot substituent (*n*Bu). Thus, the assumed pseudorotation activation barrier from **5b** to **A** is already smaller than the relative energy between **5b** and **A** by about 2 (12 – 10) kcal mol^{-1} as the lower limit. Therefore, it is unlikely that **A** exists as an energy minimum; it is probably a structure along the reaction pathway, or it could be that the turnstile mechanism[41] that is frequently neglected is the actual operative route.

Conclusions

In conclusion, by utilizing the Martin ligand, we have isolated and characterized the first anti-apicophilic phosphoranes *O-cis* **6**, with substituent configurations that violate the apicophilicity rule, as high-energy stereoisomers of phosphoranes *O-trans* **5** with an ordinary O_{apical},$C_{equatorial}$ array. This was only possible because the phosphoranes *O-cis* **6** can be formed under non-equilibration (kinetic) conditions from **10**, and because the barrier of pseudorotation for these pseudorotamers to their more stable stereoisomers *O-trans* **5** is sufficiently high enough to freeze the conversion and allow isolation. During the course of these studies we have also found that monocyclic P–H_{apical} phosphoranes **10**, which are precursors to *O-cis* **6**, exist as mixtures of solvated and unsolvated species. A ligand-exchange process interconverting the bidentate Martin ligand with the monodentate Martin ligand was found to exist. This process likely proceeds via hexacoordinate transition states. In addition, a rationale of the cyclization reaction to produce *O-cis* **6** has been presented on the basis of a kinetic examination of the process. The energy difference between *O-trans* **5** and *O-cis* **6** (R = *n*Bu) was elucidated to be about 12 kcal mol^{-1} from kinetic measurements of the transformation of *O-cis* **6** to *O-trans* **5** and between the interconversion of diastereomeric analogs of *O-trans* **5**. This is in good agreement with the calculated difference of 14.1 kcal mol^{-1} between *O-trans* **5** and *O-cis* **6** (R = Me).

Experimental Section

General: Melting points were measured with a Yanaco micro melting point apparatus and are uncorrected. ^{1}H (400 MHz), ^{13}C (100 MHz), ^{19}F (376 MHz), and ^{31}P NMR (162 MHz) spectra were recorded with a JEOL EX-400 spectrometer. ^{1}H NMR chemical shifts (δ) are given in ppm downfield from residual [D]chloroform (δ = 7.26 ppm). ^{13}C NMR chemical shifts (δ) are given in ppm from [D]chloroform (δ = 77.0 ppm). ^{19}F NMR chemical shifts (δ) are given in ppm downfield from external $CFCl_3$. ^{31}P NMR chemical shifts (δ) are given in ppm downfield from external 85% H_3PO_4. Elemental analyses were performed with a Perkin–Elmer 2400 CHN elemental analyzer. All reactions were carried out under N_2.

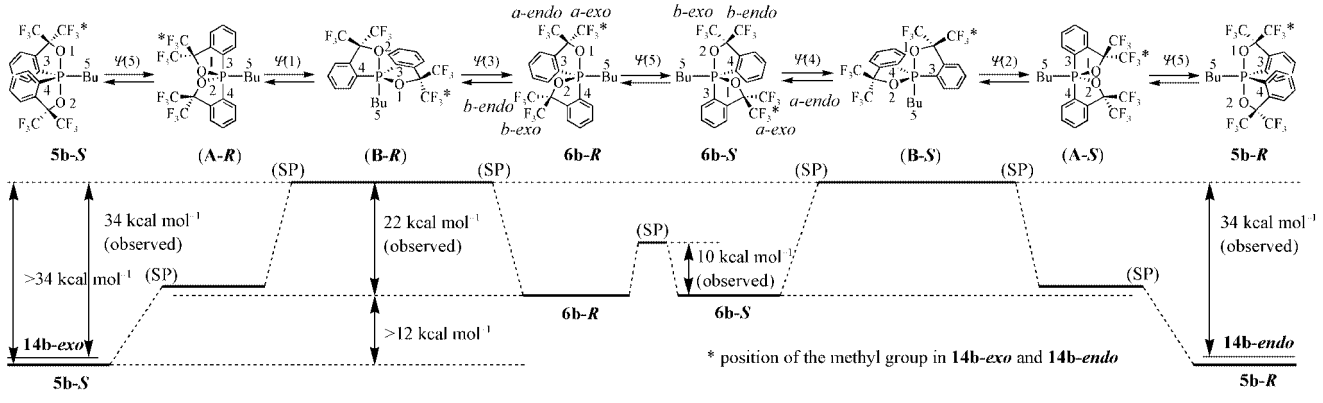

Figure 10. Energy diagram for Berry pseudorotation involving **5b**, **6b**, and **14b** (*exo* and *endo*).

THF was freshly distilled from Na/benzophenone. Ethanol was distilled from magnesium. All other solvents were distilled from CaH_2. Phosphoranes **7**[17c,20b] and **14**[8c] were prepared according to published procedures. Preparative thin layer chromatography was carried out on plates of Merck silica gel 60 GF_{254}.

[*TBPY*-5-15]-1,1,1,3,3,3-Hexafluoro-2-{2-[1-methyl-3,3-bis(trifluoromethyl)-1,3-dihydro-2,1λ^5-benzoxaphosphol-1-yl]phenyl}propan-2-ol (10a): MeLi (1.14 M in Et_2O, 5.67 mL, 6.46 mmol) was added to a solution of P–$H_{equatorial}$ phosphorane **7** (460 mg, 0.891 mmol) in Et_2O (10 mL) at –78 °C. After removal of the cooling bath, the solution was stirred at room temperature for 50 min. The solution was quenched with 1 M HCl (3 mL), extracted with Et_2O (3 × 30 mL), dried with anhydrous $MgSO_4$, and concentrated in vacuo. Separation and purification of the residue was carried out by TLC (hexane/CH_2Cl_2 = 5:1) to give **10a** (322 mg, 68%) and **5a** (105 mg, 22%) as white solids. Recrystallization of **10a** from hexane/CH_2Cl_2 gave crystals for X-ray analysis. **10a:** M.p. 101 °C. ^{1}H NMR ($CDCl_3$): δ = 8.86 (br. s, 1 H), 8.10–7.90 (m, 1 H), 7.79 (br. s, 4 H), 7.55–7.20 (m, 3 H), 6.37 (dq, $^1J_{H,P}$ = 276, $^3J_{H,H}$ = 3.9 Hz, 1 H), 2.44 (dd, $^2J_{H,P}$ = 14.7, $^3J_{H,H}$ = 3.9 Hz, 3 H) ppm. ^{13}C NMR ($CDCl_3$): δ = 136.7 (d, $^2J_{C,P}$ = 11.0 Hz), 134.8 (br. s), 133.7 (d, $^4J_{C,P}$ = 3.7 Hz), 133.5 (br. s), 131.4 (d, $^3J_{C,P}$ = 14.7 Hz), 131.1 (br. d, $^2J_{C,P}$ = 12.9 Hz), 129.8 (br. s), 129.6 (d, $^1J_{C,P}$ = 123.2 Hz), 129.1 (br. d, $^3J_{C,P}$ = 14.7 Hz), 128.3 (d, $^1J_{C,P}$ = 141.3 Hz), 128.2 (d, $^2J_{C,P}$ = 25.7 Hz), (d, $^1J_{C,F}$ = 286.8 Hz), 124.8 (d, $^3J_{C,P}$ = 14.7 Hz), 122.6 (q, $^1J_{C,F}$ = 284.8 Hz), 122.4 (q, $^1J_{C,F}$ = 290.4 Hz), 122.2 (q, $^1J_{C,F}$ = 290.5 Hz), 79.0 (sept, $^2J_{C,F}$ = 35.0 Hz), 78.9 (sept, $^2J_{C,F}$ = 33.1 Hz), 22.4 (d, $^1J_{C,P}$ = 99.3 Hz) ppm. ^{19}F NMR ($CDCl_3$): δ = –72.9 (br. s, 3 F), –76.3 (br. s, 3 F), –76.9 (br. s, 3 F), –77.0 (br. s, 3 F) ppm. ^{31}P NMR ($CDCl_3$): δ = –51.9 ppm. $C_{19}H_{13}F_{12}O_2P$ (532.26): calcd. C 42.88, H 2.46; found C 42.75, H 2.37.

[*TBPY*-5-15]-1,1,1,3,3,3-Hexafluoro-2-{2-[1-butyl-3,3-bis(trifluoromethyl)-1,3-dihydro-2,1λ^5-benzoxaphosphol-1-yl]phenyl}propan-2-ol (10b): *n*BuLi (1.62 M in hexane, 2.00 mL, 3.24 mmol) was added to a solution of P–$H_{equatorial}$ spirophosphorane **7** (500 mg, 0.969 mmol) in Et_2O (10 mL) at –78 °C. After removal of the cooling bath, the solution was stirred at room temperature for 60 min. The solution was quenched with 1 M HCl (10 mL), extracted with Et_2O (3 × 30 mL), dried with anhydrous $MgSO_4$, and concentrated in vacuo. Separation and purification of the residue was carried out by TLC (hexane/CH_2Cl_2 = 5:1) to give **10b** (322 mg, 68%) and **5b** (105 mg, 22%) as white solids. Recrystallization of **10b** from hexane/CH_2Cl_2 gave crystals suitable for X-ray analysis. **10b:** M.p. 119 °C. ^{1}H NMR ($CDCl_3$): δ = 9.13 (br. s, 1 H), 8.07–8.02 (m, 1 H), 7.89–7.85 (m, 1 H), 7.80–7.72 (m, 3 H), 7.45–7.41 (m, 1 H), 7.36–7.32 (m, 1 H), 6.16 (dd, $^1J_{H,P}$ = 273, $^3J_{H,H}$ = 5.9 Hz, 1 H), 3.21–3.06 (m, 1 H), 2.69–2.52 (m, 1 H), 1.65–1.46 (m, 1 H), 1.45–1.36 (m, 2 H), 1.35–1.22 (m, 1 H), 0.88 (t, $^3J_{H,H}$ = 7.3 Hz, 3 H) ppm. ^{13}C NMR ($CDCl_3$): δ = 136.6 (d, $^2J_{C,P}$ = 12.8 Hz), 136.1 (d, $^1J_{C,P}$ = 139.7 Hz), 134.7, 134.3 (d, $^3J_{C,P}$ = 14.7 Hz), 134.1 (d, $^3J_{C,P}$ = 14.7 Hz), 130.8 (d, $^2J_{C,P}$ = 16.5 Hz), 130.2, 129.8 (d, $^1J_{C,P}$ = 139.7 Hz), 129.7, 129.1 (d, $^2J_{C,P}$ = 16.6 Hz), 127.0 (d, $^3J_{C,P}$ = 12.9 Hz), 123.4 (d, $^1J_{C,F}$ = 290.4 Hz), 122.7 (q, $^1J_{C,F}$ = 286.8 Hz), 122.5 (q, $^1J_{C,F}$ = 286.8 Hz), 122.3 (q, $^1J_{C,F}$ = 288.6 Hz), 78.9 (sept, $^2J_{C,F}$ = 31.2 Hz), 78.6 (sept, $^2J_{C,F}$ = 31.2 Hz), 34.7 (d, $^1J_{C,P}$ = 90.1 Hz), 27.7, 23.5 (d, $^2J_{C,P}$ = 23.9 Hz), 13.6 ppm. ^{19}F NMR ($CDCl_3$): δ = –72.9 (br. s, 3 F), –76.3 (q, $^4J_{F,F}$ = 9.2 Hz, 3 F), –76.8 (q, $^4J_{F,F}$ = 8.2 Hz, 3 F), –77.0 (q, $^4J_{F,F}$ = 9.2, $^9J_{F,F}$ = 4.9 Hz, 3 F) ppm. ^{31}P NMR ($CDCl_3$): δ = –34.4 ppm. $C_{22}H_{19}F_{12}O_2P$ (574.34): calcd. C 46.01, H 3.33; found C 46.09, H, 3.24.

[*TBPY*-5-15]-1,1,1,3,3,3-Hexafluoro-2-{2-[1-(1,1-dimethylethyl)-3,3-bis(trifluoromethyl)-1,3-dihydro-2,1λ^5-benzoxaphosphol-1-yl]phenyl}propan-2-ol (10c): *t*BuLi (1.70 M in pentane, 3.60 mL, 6.12 mmol) was added to a solution of P–$H_{equatorial}$ spirophosphorane **7** (1.00 mg, 1.94 mmol) in Et_2O (20 mL) at –78 °C. After removal of the cooling bath, the solution was stirred at room temperature for 30 min. The solution was quenched with 1 M HCl (20 mL), extracted with Et_2O (3 × 50 mL), dried with anhydrous $MgSO_4$, and concentrated in vacuo. Separation and purification of the residue was carried out by TLC (hexane/CH_2Cl_2 = 5:1) to give a mixture (1.01 g, 92%) of **10c$_{intra}$** and **10c$_{inter}$** as a white powder. Recrystallization from hexane/CCl_4 gave crystals of **10c$_{intra}$**. **10c$_{intra}$:** M.p. 108 °C. ^{1}H NMR ($CDCl_3$): δ = 8.58 (br. s, 1 H), 8.00–7.89 (m, 1 H), 7.80–7.48 (m, 7 H), 5.81 (d, $^1J_{H,P}$ = 273 Hz, 1 H), 1.30 (d, $^3J_{H,P}$ = 23.4 Hz, 9 H) ppm. ^{13}C NMR ($CDCl_3$): δ = 139.3 (d, $^1J_{C,P}$ = 139.7 Hz), 136.7 (d, $^1J_{C,P}$ = 132.4 Hz), 136.2 (d, $^3J_{C,P}$ = 16.6 Hz), 134.6 (d, $^3J_{C,P}$ = 12.9 Hz), 134.0, 131.3 (d, $^2J_{C,P}$ = 14.7 Hz), 130.6 (d, $^2J_{C,P}$ = 14.7 Hz), 129.5, 129.2 (d, $^2J_{C,P}$ = 16.6 Hz), 129.0, 128.8 (d, $^3J_{C,P}$ = 3.9 Hz), 126.5 (d, $J_{C,P}$ = 16.6 Hz), 123.4 (q, $^1J_{C,F}$ = 286.8 Hz), 123.1 (q, $^1J_{C,F}$ = 290.4 Hz), 122.7 (q, $^1J_{C,F}$ = 288.6 Hz), 122.3 (q, $^1J_{C,F}$ = 288.6 Hz), 79.7 (sept, $^2J_{C,F}$ = 31.3 Hz), 78.4 (sept, $^2J_{C,F}$ = 31.3 Hz), 43.8 (d, $^1J_{C,P}$ = 90.1 Hz), 15.1 ppm. ^{19}F NMR ($CDCl_3$): δ = –73.4 (q, $^4J_{F,F}$ = 9.5 Hz, 3 F), –73.5 (q, $^4J_{F,F}$ = 9.5 Hz, 3 F), –74.6 (q, $^4J_{F,F}$ = 9.1 Hz, 3 F), –76.1 (q, $^4J_{F,F}$ = 10.7 Hz, 3 F) ppm. ^{31}P NMR ($CDCl_3$): δ = –14.7 ppm. $C_{22}H_{19}F_{12}O_2P$ (574.34): calcd. C 46.01, H 3.33; found C 45.85, H, 3.23. Recrystallization from hexane/EtOH gave crystals of **10c$_{inter}$** (containing EtOH). An X-ray sample was recrystallized from hexane/MeCN. **10c$_{inter}$:** M.p. 83–84 °C (containing EtOH). ^{1}H NMR ([D$_6$]acetone, without EtOH): δ = 8.77–8.72 (m, 1 H), 7.87–7.82 (m, 1 H), 7.75–7.63 (m, 4 H), 7.63–7.54 (m, 2 H), 7.48 (s, 1 H), 6.07 (d, $^1J_{H,P}$ = 293 Hz, 1 H), 1.17 (d, $^3J_{H,P}$ = 19.5 Hz, 9 H) ppm. ^{13}C NMR ([D$_6$]acetone, without EtOH): δ = 141.3 (d, $^1J_{C,P}$ = 141.3 Hz), 139.0 (d, $^4J_{C,P}$ = 5.5 Hz), 137.1 (d, $^2J_{C,P}$ = 14.7 Hz), 136.1 (d, $^3J_{C,P}$ = 14.7 Hz), 135.1 (d, $^1J_{C,P}$ = 139.7 Hz), 133.9, 132.7 (d, $^2J_{C,P}$ = 3.6 Hz), 130.7, 130.1 (d, $^2J_{C,P}$ = 12.9 Hz), 128.6 (d, $^3J_{C,P}$ = 7.4 Hz), 125.9 (d, $^3J_{C,P}$ = 12.9 Hz), 125.2 (q, $^1J_{C,F}$ = 286.8 Hz), 124.7 (q, $^1J_{C,F}$ = 288.6 Hz), 124.6 (q, $^1J_{C,F}$ = 290.5 Hz), 122.3 (q, $^1J_{C,F}$ = 288.7 Hz), 81.0 (sept, $^2J_{C,F}$ = 29.5 Hz), 80.0 (sept, $^2J_{C,F}$ = 29.4 Hz), 38.6 (d, $^1J_{C,P}$ = 97.5 Hz), 19.4 ppm. ^{19}F NMR ([D$_6$]acetone, without EtOH): δ = –73.3 (qq, $^4J_{F,F}$ = 8.9, $^9J_{F,F}$ = 3.1 Hz, 3 F), –73.6 (q, $^4J_{F,F}$ = 9.5 Hz, 3 F), –74.3 (q, $^4J_{F,F}$ = 8.6 Hz, 3 F), –75.5 (qq, $^4J_{F,F}$ = 9.2, $^9J_{F,F}$ = 2.8 Hz, 3 F) ppm. ^{31}P NMR ([D$_6$]-acetone, without EtOH): δ = –40.1 ppm. $C_{24}H_{25}F_{12}O_3P$ (620.41): calcd. C 46.46, H 4.06 (containing EtOH); found C 46.26, H, 3.90.

[*TBPY*-5-12]-1-Methyl-3,3,3′,3′-tetrakis(trifluoromethyl)-1,1′-spirobi[1,3-dihydro-2,1λ^5-benzoxaphosphole] (6a): A solution of P–H_{apical} phosphorane **10a** (50 mg, 9.4×10^{-2} mmol) in THF (0.5 mL) was heated at 40 °C for 1 h. The solution was concentrated in vacuo. Purification of the residue was carried out by TLC (hexane/CH_2Cl_2 = 2:1) to give **5a** (R_f = 0.8, 23 mg, 46%) and **6a** (R_f = 0.9, 26 mg, 52%) as white solids. **5a:** M.p. 134 °C. ^{1}H NMR ($CDCl_3$): δ = 8.43–8.38 (m, 2 H), 7.79–7.69 (m, 6 H), 2.11 (d, $^2J_{H,P}$ = 16.6 Hz, 3 H) ppm. ^{13}C NMR ($CDCl_3$): δ = 136.8 (d, $^3J_{C,P}$ = 9.1 Hz), 136.1 (d, $^2J_{C,P}$ = 20.2 Hz), 133.7 (d, $^4J_{C,P}$ = 3.7 Hz), 131.4 (d, $^2J_{C,P}$ = 14.7 Hz), 130.6 (d, $^1J_{C,P}$ = 176.5 Hz), 124.8 (d, $^3J_{C,P}$ = 14.7 Hz), 122.6 (q, $^1J_{C,F}$ = 285.0 Hz), 122.4 (q, $^1J_{C,F}$ = 288.6 Hz), 81.3 (sept, $^2J_{C,F}$ = 31.2 Hz), 25.2 (d, $^1J_{C,P}$ = 125.0 Hz) ppm. ^{19}F NMR ($CDCl_3$): δ = –75.1 (q, $^4J_{F,F}$ = 9.5 Hz, 6 F), –75.4 (q, $^4J_{F,F}$ = 9.5 Hz, 6 F) ppm. ^{31}P NMR ($CDCl_3$): δ = –22.6 ppm. $C_{19}H_{11}F_{12}O_2P$ (530.24): calcd. C 43.04, H 2.09; found C 42.83, H 1.86. **6a:** M.p. 127 °C. ^{1}H NMR ($CDCl_3$): δ = 7.80–7.31 (m, 8 H), 2.28 (d, $^2J_{H,P}$ = 10.2 Hz, 3 H) ppm. ^{13}C NMR ($CDCl_3$): δ = 136.8 (d, $J_{C,P}$ = 9.1 Hz), 136.1 (d, $J_{C,P}$ = 20.2 Hz), 133.8 (d, $J_{C,P}$ = 3.7 Hz), 132.3 (br. s), 132.0 (br. s), 131.4 (d, $J_{C,P}$ = 14.7 Hz), 130.3 (d, $J_{C,P}$ =

11.1 Hz), 125.6 (d, $J_{C,P}$ = 9.1 Hz), 124.8 (d, $J_{C,P}$ = 14.7 Hz), 122.6 (q, $^1J_{C,F}$ = 285.0 Hz), 122.4 (q, $^1J_{C,F}$ = 288.6 Hz), 122.3 (q, $^1J_{C,F}$ = 285.9 Hz), 121.9 (q, $^1J_{C,F}$ = 285.8 Hz), 79.8 (sept, $^2J_{C,F}$ = 31.3 Hz), 26.2 (d, $^1J_{C,P}$ = 129.5 Hz) ppm. ^{19}F NMR ($CDCl_3$): δ = –75.6 (q, $^4J_{F,F}$ = 9.2 Hz, 6 F), –76.4 (q, $^4J_{F,F}$ = 8.6 Hz, 6 F) ppm. ^{31}P NMR ($CDCl_3$): δ = –6.3 ppm. $C_{19}H_{11}F_{12}O_2P$ (530.24): calcd. C 43.04, H 2.09; found C 43.34, H 1.99.

[*TBPY*-5-12]-1-Butyl-3,3,3′,3′-tetrakis(trifluoromethyl)-1,1′-spirobi-[1,3-dihydro-2,1λ^5-benzoxaphosphole] (6b): P–H_{apical} phosphorane **10b** (200 mg, 0.348 mmol) was treated with pyridine (0.07 mL, 0.8 mmol) in THF (5 mL) at 60 °C for 20 min. The solution was quenched with 1 M HCl (50 mL), extracted with Et_2O (50 mL), and washed with aqueous $CuSO_4$ (50 mL), water (50 mL), and brine (50 mL). The mixture was then dried with $MgSO_4$, and concentrated in vacuo. Purification of the residue was carried out by TLC (hexane/CH_2Cl_2 = 2:1) to give **5b** (R_f = 0.9, 58.2 mg, 29%) and **6b** (R_f = 0.7, 141 mg, 71%) as white solids. Recrystallization of **5b** and **6b** from MeCN gave single crystals suitable for X-ray analysis. **5b:** M.p. 109 °C. ^{1}H NMR ($CDCl_3$): δ = 8.43–8.38 (m, 2 H), 7.72–7.58 (m, 6 H), 2.34 (ddt, $^2J_{H,P}$ = 28.3, $^2J_{H,H}$ = 12.2, $^3J_{H,H}$ = 4.9 Hz, 1 H), 2.20 (ddt, $^2J_{H,P}$ = 12.2, $^2J_{H,H}$ = 12.2, $^3J_{H,H}$ = 4.4 Hz, 1 H), 1.86–1.70 (m, 1 H), 1.32–1.20 (m, 3 H), 0.81 (t, $^3J_{H,H}$ = 7.3 Hz, 3 H) ppm. ^{13}C NMR ($CDCl_3$): δ = 137.1 (d, $^3J_{C,P}$ = 9.2 Hz), 136.2 (d, $^2J_{C,P}$ = 18.4 Hz), 133.6 (d, $^4J_{C,P}$ = 3.6 Hz), 131.3 (d, $^2J_{C,P}$ = 14.7 Hz), 130.3 (d, $^1J_{C,P}$ = 160.0 Hz), 124.8 (d, $^3J_{C,P}$ = 14.7 Hz), 122.7 (q, $^1J_{C,F}$ = 286.8 Hz), 122.5 (q,$^1J_{C,F}$ = 290.5 Hz), 81.3 (sept, $^2J_{C,F}$ = 31.2 Hz), 39.2 (d, $^1J_{C,P}$ = 115.8 Hz), 25.3 (d, $^3J_{C,P}$ = 7.4 Hz), 23.6 (d, $^2J_{C,P}$ = 23.9 Hz), 13.2 ppm. ^{19}F NMR ($CDCl_3$): δ = –75.1 (q, $^4J_{F,F}$ = 9.3 Hz, 6 F), –75.4 (q, $^4J_{F,F}$ = 9.3 Hz, 6 F) ppm. ^{31}P NMR ($CDCl_3$): δ = –18.8 ppm. $C_{22}H_{17}F_{12}O_2P$ (572.32): calcd. C 46.17, H 2.99; found C 46.19, H 2.84. **6b:** M.p. 115 °C. ^{1}H NMR ($CDCl_3$): δ = 7.75–7.69 (m, 2 H), 7.67–7.65 (m, 2 H), 7.59–7.56 (m, 4 H), 2.48 (dt, $^2J_{H,P}$ = 17.1, $^3J_{H,H}$ = 6.8 Hz, 2 H), 1.67–1.54 (m, 2 H), 1.39–1.29 (m, 2 H), 0.83 (t, $^3J_{H,H}$ = 7.3 Hz, 3 H) ppm. ^{13}C NMR ($CDCl_3$): δ = 135.9 (br. d, $^1J_{C,P}$ = 88.3 Hz), 134.2 (d, $^2J_{C,P}$ = 16.5 Hz), 132.2, 132.0 (d, $^3J_{C,P}$ = 11.1 Hz), 130.3 (d, $^2J_{C,P}$ = 11.1 Hz), 125.5 (d, $^3J_{C,P}$ = 11.0 Hz), 122.5 (d, $^3J_{C,P}$ = 7.4 Hz), 122.5 (q, $^1J_{C,F}$ = 286.8 Hz), 122.0 (q, $^1J_{C,F}$ = 288.8 Hz), 79.9 (sept, $^2J_{C,F}$ = 31.3 Hz), 40.2 (d, $^1J_{C,P}$ = 114.0 Hz), 24.7 (d, $^3J_{C,P}$ = 7.4 Hz), 24.0 (d, $^2J_{C,P}$ = 20.2 Hz), 13.3 ppm. ^{19}F NMR ($CDCl_3$): δ = –74.9 (q, $^4J_{F,F}$ = 8.5 Hz, 6 F), –76.2 (q, $^4J_{F,F}$ = 8.5 Hz, 6 F) ppm. ^{31}P NMR ($CDCl_3$): δ = –3.5 ppm. $C_{22}H_{17}F_{12}O_2P$ (572.32): calcd. C 46.17, H 2.99; found C 46.17, H 2.72.

[*TBPY*-5-11]-1-(1,1-Dimethylethyl)-3,3,3′,3′-tetrakis(trifluoromethyl)-1,1′-spirobi[1,3-dihydro-2,1λ^5-benzoxaphosphole] (5c): A solution of P–H_{apical} phosphorane **10c** (150 mg, 0.261 mmol) in *o*-dichlorobenzene (10 mL) and CH_3CN (2 mL) was heated at 150 °C for 4 d. The solution was then concentrated in vacuo. Purification of the residue was carried out by TLC (hexane) to give **5c** (R_f = 0.8, 224 mg, 80%) as a white solid. Recrystallization from hexane gave an X-ray sample. M.p. 128 °C. ^{1}H NMR ($CDCl_3$): δ = 8.42–8.38 (m, 2 H), 7.66–7.64 (m, 6 H), 1.13 (d, $^3J_{H,P}$ = 20.0 Hz, 9 H) ppm. ^{13}C NMR ($CDCl_3$): δ = 137.2 (d, $^3J_{C,P}$ = 9.2 Hz), 136.4 (d, $^2J_{C,P}$ = 16.6 Hz), 132.9 (d, $^4J_{C,P}$ = 3.7 Hz), 132.5 (d, $^1J_{C,P}$ = 160.0 Hz), 130.9 (d, $^2J_{C,P}$ = 12.8 Hz), 124.1 (q, $^3J_{C,P}$ = 14.7 Hz), 122.7 (q, $^1J_{C,F}$ = 286.7 Hz), 122.4 (q, $^1J_{C,F}$ = 288.6 Hz), 81.5 (sept, $^2J_{C,F}$ = 31.3 Hz), 40.5 (d, $^1J_{C,P}$ = 103.0 Hz), 28.2 ppm. ^{19}F NMR ($CDCl_3$): δ = –72.4 (q, $^4J_{F,F}$ = 10.1 Hz, 6 F), –74.5 (q, $^4J_{F,F}$ = 10.1 Hz, 6 F) ppm. ^{31}P NMR ($CDCl_3$): δ = –9.8 ppm. $C_{22}H_{17}F_{12}O_2P$: calcd. C 46.17, H 2.99; found C 46.04, H 2.73.

[*TBPY*-5-12]-1-(1,1-Dimethylethyl)-3,3,3′,3′-tetrakis(trifluoromethyl)-1,1′-spirobi[1,3-dihydro-2,1λ^5-benzoxaphosphole] (6c): P–H_{apical} phosphorane **10c** (300 mg, 0.523 mmol) was treated with pyridine (4.0 mL, 0.8 mmol) in THF (20 mL) at 60 °C for 36 h. The solution was quenched with 1 M HCl (50 mL), extracted with Et_2O (50 mL), and washed with aqueous $CuSO_4$ (50 mL), water (50 mL), and brine (50 mL). The mixture was then dried with $MgSO_4$, and concentrated in vacuo. Purification of the residue was carried out by TLC (hexane/CH_2Cl_2 = 3:1) to give **6c** (R_f = 0.6, 224 mg, 75%) and **10c** (R_f = 0.4, 53.7 mg, 18% recovery) as white solids. Recrystallization of **6c** from EtOH gave an X-ray sample. M.p. 138 °C. ^{1}H NMR ($CDCl_3$): δ = 7.91–7.88 (m, 2 H), 7.73–7.71 (m, 2 H), 7.62–7.52 (m, 4 H), 1.21 (d, $^3J_{H,P}$ = 21.0 Hz, 9 H) ppm. ^{13}C NMR ($CDCl_3$): δ = 136.3 (d, $^1J_{C,P}$ = 77.2 Hz), 134.1 (d, $^2J_{C,P}$ = 14.7 Hz), 133.8 (d, $^2J_{C,P}$ = 12.9 Hz), 131.7, 129.4 (d, $^3J_{C,P}$ = 9.2 Hz), 125.4 (d, $^3J_{C,PP}$ = 9.2 Hz), 122.64 (q, $^1J_{C,F}$ = 286.8 Hz), 122.57 (q, $^1J_{C,F}$ = 286.8 Hz), 122.0 (q, $^1J_{C,F}$ = 288.6 Hz), 79.6 (sept, $^2J_{C,F}$ = 31.2 Hz), 44.4 (d, $^1J_{C,P}$ = 112.1 Hz), 29.6 ppm. ^{19}F NMR ($CDCl_3$): δ = –73.7 (q, $^4J_{F,F}$ = 9.2 Hz, 6 F), –75.9 (q, $^4J_{F,F}$ = 9.5 Hz, 6 F) ppm. ^{31}P NMR ($CDCl_3$): δ = 7.7 ppm. $C_{22}H_{17}F_{12}O_2P$ (572.32): calcd. C 46.17, H 2.99; found C 46.32, H 3.27.

X-ray Crystal Structure Determination of 10a, 10b, 10c$_{intra}$, 10c$_{inter}$, and 6c: Crystals suitable for X-ray structure determination were mounted on a Mac Science MXC3 diffractometer and irradiated with graphite-monochromated Cu-K_α radiation (λ = 1.54178 Å) for data collection for **10b**, **10c$_{intra}$**, and **6c**, and graphite-monochromated Mo-K_α radiation (λ = 0.71073 Å) for data collection for **10a** and **10c$_{inter}$**. Lattice parameters were determined by least-squares fitting of 31 reflections for all compounds with $51° < 2\theta < 60°$. Data were collected in the $2\theta/\omega$ scan mode. All data were corrected for absorption[42] and extinction.[43] The structures were solved by direct methods and refined by full-matrix least-squares methods with the teXsan program.[44] All non-hydrogen atoms were refined with anisotropic thermal parameters. All hydrogen atoms in **6c** and the hydrogen atoms directly attached to P1 and O2 were located from a difference Fourier map calculated at the final or at a late stage of the structural analysis. All other hydrogen atoms were included in the refinement at calculated positions (C–H = 1.0 Å) riding on their carrier atoms with isotropic thermal parameters. CCDC-258229 (**6c**), -258230 (**10a**), -258231 (**10b**), -258232 (**10c$_{intra}$**), and -258233 (**10c$_{inter}$**) contain the supplementary crystallographic data for this paper. These data can be obtained free of charge from The Cambridge Crystallographic Data Centre via www.ccdc.cam.ac.uk/data_request/cif.

Dynamic NMR Measurements: Samples of **10b** and **6b** (ca. 15 mg), dissolved in freshly distilled solvent (0.5–0.6 mL), were sealed separately in NMR tubes under N_2. ^{19}F NMR spectra were measured in a variable-temperature mode (error within ±1 °C). The observed temperatures were calibrated with the ^{1}H NMR chemical shift difference of signals of neat 1,3-propanediol (high-temperature region) and MeOH (low-temperature region). The rates and activation free energies at the coalescence point were calculated using the Gutowsky–Holm approximation method and the line-shape analysis was performed in a narrow temperature range around the coalescence point The activation enthalpies and entropies were calculated according to the transition state theory of Eyring by linear regression.

Kinetic Measurements of the Pseudorotation of 6b and 6c, and Cyclization of 10b and 10c: Samples (ca. 15 mg), dissolved in freshly distilled solvent (0.5–0.6 mL), were separately sealed in NMR tubes under N_2. For pseudorotation of **6b** and cyclization of **10b** and **10c** (in pyridine), ^{19}F NMR spectra were measured in a variable-temperature mode, and the specified temperatures were maintained throughout each set of measurements (error within ±1 °C). For the

cyclization of **10c** in solvents other than pyridine, the ^{31}P NMR spectra were monitored in a broad-band decoupling mode. Integrals of ^{31}P signals were confirmed to be proportional to the amount of compounds by ^{19}F NMR spectroscopy. For the observation of the pseudorotation of **6c**, ^{19}F NMR spectra were measured at room temp. after heating samples at specified temperatures for arbitrary periods of time. The temperatures were maintained with a silicon oil bath (error within ±2 °C). The data for those other than **10b** in pyridine, were analyzed by assuming irreversible first-order kinetics using the equation $\ln (c_0/c) = kT$, in which c_0 = concentration of reactant at $t = 0$ and c = concentration of reactant at arbitrary intervals. For **10b** in pyridine, analysis was carried out by assuming a combination of irreversible first-order competitive and consecutive reactions (see text).

Supporting Information (see footnote on first page of this article): Crystallographic data for **10a**, **10b**, $\mathbf{10c_{inter}}$, $\mathbf{10c_{intra}}$, and **6c**, and ORTEP drawings of **10a**, **10b**, and **6c**.

Acknowledgments

The authors are grateful to Central Glass Co. Ltd. for a generous gift of hexafluorocumyl alcohol. Partial support of this work through Grants-in-Aid for Scientific Research (nos. 06740488 and 07740501) provided by the Ministry of Education, Science, and Culture of the Japanese Government is heartily acknowledged.

[1] For the *N-X-L* designation, see: C. W. Perkins, J. C. Martin, A. J. Arduengo, W. Lau, A. Alegria, J. K. Kochi, *J. Am. Chem. Soc.* **1980**, *102*, 7753–7759.
[2] a) F. H. Westheimer, *Acc. Chem. Res.* **1968**, *1*, 70–78; b) G. R. J. Thatcher, R. Kluger, *Adv. Phys. Org. Chem.* **1989**, *25*, 99–265 and references cited therein.
[3] R. S. Berry, *J. Chem. Phys.* **1960**, *32*, 933–938.
[4] a) R. R. Holmes, *Pentacoordinated Phosphorus − Structure and Spectroscopy*, ACS Monographs 175 and 176, American Chemical Society, Washington, DC, **1980**, vols. I and II; b) N. A. Polezhaeva, R. A. Cherkasoz, *Usp. Khim.* **1985**, *54*, 1899–1939; c) L. N. Markovskii, N. P. Kolesnik, Y. G. Shermolovich, *Usp. Khim.* **1987**, *56*, 1564–1583; d) R. Burgada, R. Setton, in *The Chemistry of Organophosphorus Compounds* (Ed.: F. R. Hartley), Wiley-Interscience, Chichester, **1994**, pp. 185–272; e) K.-y. Akiba, *Chemistry of Hypervalent Compounds*, Wiley-VCH, New York, **1999**.
[5] a) G. C. Pimentel, *J. Chem. Phys.* **1951**, *19*, 446–448; b) R. J. Hach, R. E. Rundle, *J. Am. Chem. Soc.* **1951**, *73*, 4321–4324; c) J. I. Musher, *Angew. Chem. Int. Ed. Engl.* **1969**, *8*, 54–68.
[6] E. L. Muetteries, W. Mahler, R. Schmutzler, *Inorg. Chem.* **1963**, *2*, 613–618.
[7] a) S. Trippett, *Phosphorus Sulfur* **1976**, *1*, 89–98; b) M. Eisenhut, H. L. Mitchell, D. D. Traficante, R. J. Kaufman, J. M. Deutsch, G. M. Whitesides, *J. Am. Chem. Soc.* **1974**, *96*, 5385–5397; c) C. G. Moreland, G. O. Doak, L. B. Littlefield, N. S. Walker, J. W. Gilje, R. W. Braun, A. H. Cowley, *J. Am. Chem. Soc.* **1976**, *98*, 2161–2165; d) G. Buono, J. R. Llinas, *J. Am. Chem. Soc.* **1981**, *103*, 4532–4540; e) L. V. Griend, R. G. Cavell, *Inorg. Chem.* **1983**, *22*, 1817–1820.
[8] a) S. Kojima, M. Nakamoto, K. Kajiyama, K.-y. Akiba, *Tetrahedron Lett.* **1995**, *36*, 2261–2264; b) S. Kojima, M. Nakamoto, K. Yamazaki, K.-y. Akiba, *Tetrahedron Lett.* **1997**, *38*, 4107–4110; c) M. Nakamoto, S. Kojima, S. Matsukawa, Y. Yamamoto, K.-y. Akiba, *J. Organomet. Chem.* **2002**, *643–644*, 441–452; d) S. Matsukawa, K. Kajiyama, S. Kojima, S.-y. Furuta, Y. Yamamoto, K.-y. Akiba, *Angew. Chem. Int. Ed.* **2002**, *41*, 4718–4722.
[9] a) H. J. Bestmann, J. Chandrasekhar, W. G. Downey, P. v. R. Schleyer, *J. Chem. Soc., Chem. Commun.* **1980**, 978–979; b) R. S. McDowell, A. Streitwieser, Jr., *J. Am. Chem. Soc.* **1985**, *107*, 5849–5855; c) P. Wang, Y. Zhang, R. Glaser, A. E. Reed, P. v. R. Schleyer, A. Streitwieser, *J. Am. Chem. Soc.* **1991**, *113*, 55–64; d) G. R. J. Thatcher, A. S. Campbell, *J. Org. Chem.* **1993**, *58*, 2272–2281.
[10] R. R. Holmes, *J. Am. Chem. Soc.* **1978**, *100*, 433–446.
[11] H. Wasada, K. Hirao, *J. Am. Chem. Soc.* **1992**, *114*, 16–27.
[12] P. Wang, Y. Zhang, R. Glaser, A. Streitwieser, P. v. R. Schleyer, *J. Comput. Chem.* **1993**, *14*, 522–529.
[13] O. Lösking, H. Willner, H. Oberhammer, J. Grobe, D. L. Van, *Inorg. Chem.* **1992**, *31*, 3423–3427 and references cited therein.
[14] a) R. K. Oram, S. Trippett, *J. Chem. Soc., Perkin Trans. 1* **1973**, 1300–1310; b) S. A. Bone, S. Trippett, M. W. White, P. J. Whittle, *Tetrahedron Lett.* **1974**, *15*, 1795–1798.
[15] a) N. V. Timosheva, T. K. Prakasha, A. Chandrasekaran, R. O. Day, R. R. Holmes, *Inorg. Chem.* **1995**, *34*, 4525–4526; b) N. V. Timosheva, A. Chandrasekaran, T. K. Prakasha, R. O. Day, R. R. Holmes, *Inorg. Chem.* **1996**, *35*, 6552–6560.
[16] a) T. Kawashima, T. Soda, K. Kato, R. Okazaki, *Phosphorus Sulfur Silicon Relat. Elem.* **1996**, *109–110*, 489–492; b) T. Kawashima, T. Soda, K. Kato, R. Okazaki, *Angew. Chem. Int. Ed. Engl.* **1996**, *35*, 1096–1098.
[17] a) I. Granoth, J. C. Martin, *J. Am. Chem. Soc.* **1979**, *101*, 4618–4622; I. Granoth, J. C. Martin, *J. Am. Chem. Soc.* **1979**, *101*, 4623–4626; b) E. F. Perozzi, R. S. Michalak, G. D. Figuly, W. H. Stevenson III, D. B. Dess, M. R. Ross, J. C. Martin, *J. Org. Chem.* **1981**, *46*, 1049–1053; c) M. R. Ross, J. C. Martin, *J. Am. Chem. Soc.* **1981**, *103*, 1234–1235; d) W. H. Stevenson III, S. Wilson, J. C. Martin, W. B. Farnham, *J. Am. Chem. Soc.* **1985**, *107*, 6340–6352; e) J. C. Martin, *Science* **1983**, *221*, 509–514; f) S. K. Chopra, J. C. Martin, *Heteroat. Chem. Heteroat. Chem. Heteroatom Chem.* **1991**, *2*, 71–79; g) C. D. Moon, S. K. Chopra, J. C. Martin, in *Phosphorus Chemistry, Developments in American Science* (Eds.: E. N. Walsh, E. J. Griffiths, R. W. Parry, L. D. Quin), ACS Symposium Series 486, American Chemical Society, Washington, DC, **1992**, pp. 128–136.
[18] For preliminary communications, see: a) K. Kajiyama, S. Kojima, K.-y. Akiba, *Tetrahedron Lett.* **1996**, *37*, 8409–8412; b) S. Kojima, K. Kajiyama, M. Nakamoto, K.-y. Akiba, *J. Am. Chem. Soc.* **1996**, *118*, 12866–12867.
[19] a) K. Kajiyama, M. Yoshimune, M. Nakamoto, S. Matsukawa, S. Kojima, Y. Yamamoto, K.-y. Akiba, *Org. Lett.* **2001**, *3*, 1873–1875; b) S. Kojima, M. Sugino, M. Nakamoto, S. Matsukawa, K.-y. Akiba, *J. Am. Chem. Soc.* **2002**, *124*, 7674–7675; c) S. Matsukawa, S. Kojima, K. Kajiyama, M. Nakamoto, Y. Yamamoto, K.-y. Akiba, S.-Y. Re, S. Nagase, *J. Am. Chem. Soc.* **2002**, *124*, 13154–13170.
[20] a) S. Kojima, K. Kajiyama, K.-y. Akiba, *Tetrahedron Lett.* **1994**, *35*, 7037–7040; b) S. Kojima, K. Kajiyama, K.-y. Akiba, *Bull. Chem. Soc. Jpn.* **1995**, *68*, 1785–1797.
[21] For other examples of P–H_{apical} phosphoranes see: a) G.-V. Röschenthaler, R. Bohlen, D. Z. Schomburg, *Z. Naturforsch., Teil B* **1985**, *40*, 1593–1596; b) R. A. Kemp, *Phosphorus Sulfur Silicon, Relat. Elem.* **1994**, *87*, 83–92.
[22] a) K.-y. Akiba, H. Nakata, Y. Yamamoto, S. Kojima, *Chem. Lett.* **1992**, 1559–1562; b) S. Kojima, Y. Doi, M. Okuda, K.-y. Akiba, *Organometallics* **1995**, *14*, 1928–1937.
[23] a) G. Trinquier, J.-P. Daudey, G. Caruana, Y. Madaule, *J. Am. Chem. Soc.* **1984**, *106*, 4794–4799; b) J. Moc, K. Morokuma, *Inorg. Chem.* **1994**, *33*, 551–560.
[24] A. Bondi, *J. Phys. Chem.* **1964**, *68*, 441–451.
[25] For reviews on through-space coupling, see: a) J. Hilton, L. H. Sutcliffe, *Prog. Nucl. Magn. Reson. Spectrosc.* **1975**, *10*, 27–39; b) R. H. Contreras, M. A. Natiello, G. E. Scuseria, *Magn. Reson. Rev.* **1985**, *9*, 239–321; c) R. H. Contreras, J. C. Facelli, *Annu. Rep. NMR Spectrosc.* **1993**, *27*, 255–356.
[26] H. S. Gutowsky, C. H. Holm, *J. Chem. Phys.* **1956**, *25*, 1228–1234.
[27] T. L. Windus, M. S. Gordon, L. P. Davis, L. W. Burggraf, *J. Am. Chem. Soc.* **1994**, *116*, 3568–3579.

[28] For example: M. H. Abraham, P. L. Grellier, in *The Chemistry of the Metal–Carbon Bond*, vol. 2 (Eds.:F. Hartley, S. Patai), John Wiley and Sons, New York, **1985**, chapter 2.
[29] a) Y. Yamamoto, Y. Takeda, K.-y. Akiba, *Tetrahedron Lett.* **1989**, *30*, 725–728; b) Y. Yamamoto, H. Fujikawa, H. Fujishima, K.-y. Akiba, *J. Am. Chem. Soc.* **1989**, *111*, 2276–2283; c) Y. Yamamoto, K. Ohdoi, X. Chen, M. Kitano, K.-y. Akiba, *Organometallics* **1993**, *12*, 3297–3303.
[30] H. J. Cristau, F. Plenat, in *The Chemistry of Organophosphorus Compounds* (Ed.: F. R. Hartley), Wiley-Interscience, Chichester, **1994**, pp. 45–183.
[31] a) B. Tangour, C. Malavaud, M. T. Boisdon, J. Barrans, *Phosphorus Sulfur Relat. Elem.* **1988**, *40*, 33–39; b) B. Tangour, C. Malavaud, M. T. Boisdon, J. Barrans, *Phosphorus Sulfur Silicon Relat. Elem.* **1989**, *45*, 189–195; c) B. Tangour, C. Malavaud, M. T. Boisdon, J. Barrans, *Phosphorus Sulfur Silicon, Relat. Elem.* **1990**, *53*, 423–424 and references cited therein.
[32] a) M. Wieber, W. R. Hoos, *Monatsh. Chem.* **1970**, *101*, 776–781; b) M. Wieber, K. Foroughi, *Angew. Chem. Int. Ed. Engl.* **1973**, *12*, 419–420; c) C. Malavaud, J. Barrans, *Tetrahedron Lett.* **1975**, *35*, 3077–3080; d) C. Laurenco, R. Burgada, *Tetrahedron* **1976**, *32*, 2253–2255.
[33] E_T^N: Normalized solvent polarity. C. Reichardt, in *Solvents and Solvent Effects in Organic Chemistry*, 2nd ed., VCH Publishers, Weinheim, **1988**, pp 339–405.
[34] DN^N: Normalized donor number. Y. Marcus, *J. Solution Chem.* **1984**, *13*, 599–624.
[35] F. Ramirez, G. V. Loewengart, A. T. Elefteria, K. Tasaka, *J. Am. Chem. Soc.* **1972**, *94*, 3531–3536.
[36] Because of the presence of the bidentate ligand (which cannot assume equatorial,equatorial and apical,apical configurations) six configurations are possible excluding enantiomers, and the requirement of oxygen attack from directions other than *anti* to H results in 12 modes of attack of which five give C_{apical}, O_{apical}, four give C_{apical},C_{apical}, and three give O_{apical},O_{apical} isomers.
[37] For example, see: C. Reichardt, in *Solvents and Solvent Effects in Organic Chemistry*, 2nd ed., VCH Publishers, Weinheim, **1988**, pp. 121–283.
[38] β: Solvent hydrogen-bond acceptor basicity. M. J. Kamlet, J.-L. M. Abboud, M. H. Abraham, R. W. Taft, *J. Org. Chem.* **1983**, *48*, 2877–2887.
[39] K. Mislow, *Acc. Chem. Res.* **1970**, *3*, 321–331.
[40] A rough estimate would put **C** considerably higher in energy than the highest-energy SP.
[41] For leading references involving the turnstile mechanism see: a) I. Ugi, D. Marquarding, H. Klusacek, P. Gillespie, F. Ramirez, *Acc. Chem. Res.* **1971**, *4*, 288–296; b) P. Gillespie, P. Hoffman, H. Klusacek, D. Marquarding, S. Pfohl, F. Ramirez, E. A. Tsolis, I. Ugi, *Angew. Chem. Int. Ed. Engl.* **1971**, *10*, 687–715; c) F. Ramirez, I. Ugi, *Adv. Phys. Org. Chem.* **1971**, *9*, 25–126; d) R. R. Holmes, *Acc. Chem. Res.* **1972**, *5*, 296–303; e) P. Gillespie, F. Ramirez, I. Ugi, D. Marquarding, *Angew. Chem. Int. Ed. Engl.* **1973**, *12*, 91–119; f) S.-K. Shih, S. D. Peyerimhoff, R. J. Buenker, *J. Chem. Soc., Faraday Trans. 2* **1979**, *75*, 379–389; g) P. Lemmen, R. Baumgartner, I. Ugi, F. Ramirez, *Chem. Scr.* **1988**, *28*, 451–464.
[42] A. Furusaki, *Acta Crystallogr., Sect. A* **1979**, *35*, 220.
[43] C. Katayama, *Acta Crystallogr., Sect. A* **1986**, *42*, 19.
[44] teXsan: Single-Crystal Analysis Software, version 1.9, Molecular Strucuture Corporation, The Woodlands, Texas 77381, USA, **1998**. The program was previously available from Mac Science Co..

Received: July 9, 2005
Published Online: November 2, 2005

